RECYCLING STEEL SLAG AS A CEMENT ADDITIVE

by

JEFFREY N. MURPHY

B.A.Sc. (Metals and Materials Engineering), Queen's University, 1992

A THESIS IN PARTIAL FULFILLMENT OF THE

REQUIREMENTS FOR THE DEGREE OF

MASTER OF APPLIED SCIENCE

in

THE FACULTY OF GRADUATE STUDIES

Department of Metals and Materials Engineering

We accept this thesis as conforming

to the required standard

THE UNIVERSITY OF BRITISH COLUMBIA

August, 1995

In presenting this thesis in partial fulfilment of the requirements for an advanced degree at the University of British Columbia, I agree that the Library shall make it freely available for reference and study. I further agree that permission for extensive copying of this thesis for scholarly purposes may be granted by the head of my department or by his or her representatives. It is understood that copying or publication of this thesis for financial gain shall not be allowed without my written permission.

Department of Metals + Materials Engineering

The University of British Columbia
Vancouver, Canada

Date Sept 8/95

Abstract

In Canada, approximately 1 million tonnes of steel slag are produced annually, but, at the present time, there is no economic outlet for the large scale recycling of this by-product. The overall objective of this work was to determine whether steel slag might be processed into a sufficiently cementitious material to allow it to be recycled as an additive to ordinary Portland cement clinker. Blending steel slag with with clinker in a modest ratio of 1:10, it would be possible to effectively recycle all of this steelmaking by-product. Although steel slag has a composition which is similar to that of Portland cement, (consisting mainly of lime, silica, and iron oxide), there are important compositional, mineralogical, and process related differences. Steel slag has limited cementitious properties due to both a lack of tricalcium silicate and the presence of wustite solid solutions as a predominant mineral phase. Even though wustite (FeO) possesses no inherent cementitious properties, it has been shown that hematite (Fe_2O_3) will form hydraulic minerals when cooled from a slag melt. Thus, the valence state of the iron oxide in slag and cement systems will directly influence the cementitious properties of the material.

This work explores the effects of Fe oxidation state, overall composition, and cooling rate on the mineral structure, crystalline formation, and glass forming ability of several synthetic slags and one commercial BOF slag. XRD, SEM, and EDX analyses were performed on both slow cooled and quenched slags, which had been oxidized. These analyses, of both synthetic and commercial slag, suggest that the trivalent iron (Fe_2O_3) promoted both cementitious mineral formation in the slow cooled slags and glass formation in the quenched slags. The rate of cooling directly influenced the crystalline formation and mineral structure in the solidified product. The slow cooled slags tended to form highly crystalline polycomponent mineral systems, whereas the rapidly cooled granulated slags formed a predominantly amorphous material containing the primary Portland cement minerals.

This granulated slag product was blended with Portland cement in varying ratios and hydrated to form cylindrical compression specimens. The preliminary compression results indicate that, for a hydration period of 1 to 35 days, blends with a 10% slag addition had increased strength relative to that of Portland cement. Blends with 20% slag maintained the same strength as Portland cement, while those with a 45% slag addition exhibited a significant loss in strength, for the hydration period tested. Therefore, the optimization of certain slag processing conditions enhanced the cementitious nature of the material allowing it to be blended with Portland cement, (at additions of up to 20% by weight), without affecting the strength performance of the material.

Table of Contents

ABSTRACT i

Table of Contents iv

List of Figures vi

List of Tables ix

ACKNOWLEDGMENTS x

1.0 INTRODUCTION 1
- 1.1 Current Opportunities for Recycling Steel Slag 2

2.0 LITERATURE SURVEY 5
- 2.1 Chemical Composition and Mineralogy of Cements 5
- 2.2 Equilibrium Phase Diagrams Relevant to Portland Cement 8
- 2.3 Chemical Composition and Mineralogy of Steel Slag 14
- 2.4 Comparison of mineral structures of steel slag relative to Portland Cement 19
- 2.5 Steel Slag Cements 20
- 2.6 Blast Furnace Slag Cements 21
- 2.7 Glassification of Slags 22
- 2.8 Hydration of Blast Furnace Slag Cements 25

3.0 SCOPE & OBJECTIVES 28

4.0 EXPERIMENTAL PROGRAM 30
- 4.1 Experimental Procedure for Sample Preparation
- 4.2 Experimental Procedure for Hydration and Strength Tests 34

5.0 RESULTS 37
- 5.1 Mineralogical Observations 37
  - 5.1.1 XRD, EDX, and SEM Analyses of the Synthetic Mixes 40
  - 5.1.2 XRD, EDX, and SEM Analyses of the Stelco Steel Slag 55
- 5.2 Hydration Study 61
  - 5.2.1 Blended Cement Compression Test Results 62
  - 5.2.2 X-ray Diffraction Analyses of Hydrated Portland and Blended Cements 69

6.0 CONCLUSIONS 75

Table of Contents (cont.)

7.0 RECOMMENDED WORK 79

REFERENCES 81

APPENDIX I 84

List of Figures

Figure 1. Processing of steel slag as bituminous-bound aggregate for road construction 3

Figure 2. Phase equilibrium C-S-A ternary system 9

Figure 3. Alternative cementitious zones within the C-S-A ternary system 11

Figure 4. Pseudo ternary system C-CA-2CF 12

Figure 5. The ternary system C-F-S 13

Figure 6. The (a) C-F-A-S quaternary system (b) expanded 14

Figure 7. Dicalcium silicate phase transformation 16

Figure 8. The equilibrium ternary system C-F-S 17

Figure 9. Schematic free energy diagram for granulated blast furnace slag 26

Figure 10. Long term hydration of blast furnace slag 27

Figure 11. Composite crucible setup 33

Figure 12. X-ray diffraction curve - Portland cement 38

Figure 13. X-ray diffraction pattern of the main mineral phases of Portland cement 38

Figure 14. X-ray diffraction pattern of calcium alumino-ferrites 39

Figure 15. X-ray diffraction pattern of (a) quenched and (b) slow cooled SS1 46

Figure 16. X-ray diffraction pattern of (a) quenched and (b) slow cooled SS2 47

Figure 17. X-ray diffraction pattern of (a) quenched and (b) slow cooled SS3 48

Figure 18. SEM photograph of quenched SS1 49

Figure 19. SEM photograph of quenched SS2 (50X) 49

Figure 20. SEM photograph of quenched SS3 50

List of Figures (cont.)

Figure 21. SEM photograph of quenched SS2 calcium silicates in glassy matrix (1100X) 50

Figure 22. SEM photograph of quenched SS3 calciumsilicates in glassy matrix (2000X) 51

Figure 23. SEM photograph of (a) nucleation and (b) growth of calcium silicates in the glassy matrix of a quenched synthetic slag 51

Figure 24. SEM backscattered photograph of periclase in glassy matrix of quenched synthetic slag 52

Figure 25. XRD patterns indicating the influence of cooling rate on glass content (a) quenched (b) rapid cool (c) slow cooled 53

Figure 26. SEM photograph of slow cooled SS1 54

Figure 27. SEM photograph of slow cooled SS2 54

Figure 28. X-ray diffraction pattern - Stelco steel slag (a) as received and (b) oxidized at 900° C 57

Figure 29. X-ray diffraction pattern of (a) quenched and (b) slow cooled Stelco slag 58

Figure 30. SEM photograph of slow cooled Stelco steel slag 59

Figure 31. Amorphous quenched Stelco slag (a) and crystallite growth in a glassy matrix (b) 60

Figure 32. Compressive strengths of 10% steel slag blended ements 65

Figure 33. Compressive strengths of 10% steel slag blended cements 65

Figure 34. Compressive strengths of 20% steel slag blended cements 66

Figure 35. Compressive strengths of 45% steel slag blended cements 66

Figure 36. Compressive strengths versus steel slag addition 67

Figure 37. Compressive strengths of a 25% steel slag, 25% GGBFS, 10% gypsum, 40% Portland cement blended cement 68

List of Figures (cont.)

Figure 38. Compressive strengths of a 40% steel slag, 40% GGBFS, 10% gypsum, 10% Portland cement blended cement 68

Figure 39. XRD Pattern of a fully reacted 23 year old belite paste 70

Figure 40. XRD Pattern of hydrated Portland cement paste 72

Figure 41. XRD Pattern of a 10% Stelco steel slag blended cement 73

Figure 42. XRD Pattern of a 20% Stelco steel slag blended cement 74

Figure 43. Effect of slag addition on XRD traces after 1 day hydration 75

List of Tables

Table I - Weight % of Chemical Constituents 5

Table II - Predominant Minerals Associated with Steel Slag 15

Table III - Relationship between Basicity and Viscosity 24

Table IV - Steel Slag Composition (Weight %) 30

Table V - Composition of Cement Pastes 35

ACKNOWLEDGMENTS

The author wishes to express his gratitude and thanks to his research supervisors, Dr. T. R. Meadowcroft and Dr. P. V. Barr for their advice, encouragement, expertise, and patience during the course of this project. Thanks are also extended to the faculty, staff, and fellow graduate students in the Department of Metals and Materials Engineering. Financial assistance from the Cy and Emerald Keyes Foundation and the University Graduate Fellowship Award is gratefully acknowledged.

1.0 INTRODUCTION

Slag is generated by the steelmaking process at a rate of approximately 100-200 kg. per tonne of product in integrated plants using basic oxygen furnaces and 50 kg. per tonne in electric arc furnace plants (mini-mills). The total generation rate in Canada is approximately one million tonnes per year. This slag is stored indefinitely on site at some plants, shipped as fill from others, or, to a very limited extent, sold to cement manufacturers as an iron and lime raw material source. However, revenue from the sale of steel making slag is low and often there is a net cost associated with sending the material off-site. One option for the recycling of steel slag, provided a sufficiently cementitious nature can be instilled, could be as an additive to Portland cement clinker. Since such slags consist mainly of burnt lime and calcium silicates, it is a possibility that, with some beneficiation, the steel slags could be useful cement additives downstream of the energy intensive clinkering operation. To date, steel slag has been used only as a minor raw material additive in the manufacture of Portland cement, upstream of the clinkering process, because the form and variability of the chemical composition have caused difficulty in ensuring quality in the final cement product.

Attenuating the overall feed to the cement kiln is an attractive prospect for the cement manufacturer. The clinkering process is very energy intensive, requiring over 4 Gigajoules per tonne of product. During the calcination of limestone ($CaCO_3$) to lime (CaO), which is an integral part of the clinkering process, a considerable amount of CO_2 is released into the atmosphere. Moreover, the combustion of large amounts of fossil fuel to drive the clinkering process means that substantial CO_2 generation is associated with cement manufacture. These negative environmental factors could be abated by reducing the total amount of raw material to be clinkered. Approximately nine million tonnes of Portland cement are produced annually in Canada. Thus steel slag as an additive to cement clinker, in a 1:10 ratio, could

effectively recycle all of the steelmaking byproduct, while reducing the material flow through the cement clinkering kiln by 10%.

Cements can be extended, and are often beneficiated, by the addition of finely divided pozzolanic materials such as fly ash, alkali or bauxite waste, or granulated blast furnace slag. The introduction of these artificial additives, either to the natural raw materials or to the clinker, is common practice in the manufacture of cements [1]. However, with the exception of being incorporated in small amounts as a source of iron in the raw material stream, steel slag, (unlike blast furnace slag), cannot be directly blended with clinker without seriously degrading cement quality. The focus of the present work was to develop a process whereby the hydraulic properties of steel slag could be enhanced to a level which would allow direct addition to cement clinker with no loss in strength to pure Portland cement. The forgiving nature of Portland cement to the presence of impurities, and the potentially hydraulic nature of steel slag suggest that such a practice may be viable, as well as generating substantial benefits to both the steelmaker and the cement manufacturer.

1.1 Current Opportunities for Recycling of Steel Slag

The recycling of steel slag worldwide has been mainly as aggregate in road bed construction and, to a lesser extent, as a substitute for gravel on unpaved roads. Neither application involves any significant value added benefits for the steel manufacturer. The decisive criterion for the use of any material as aggregate in road construction is its volume stability *in situ* [2]. Unfortunately, the high content of free lime and magnesia generally results in rather poor volume stability of steel slag aggregate. Since steel slag is invariably basic due to the processing benefits of a substantial lime or dolomite flux, its performance as an aggregate can be unsatisfactory [3]. The presence and compositional variability of free lime and magnesia in the steelmaking slag will stem from the type of flux used by the

different steel producers. For example, a dolomite flux will result in a higher MgO content in the final slag product. Overall steel slags have been considered to vary significantly in chemical composition from producer to producer. However, with the advent of highly technological processing methods and the use of high grade ores charged to the BOF vessel, the degree of variability in the final slag product is continually decreasing resulting in a more standardized product [2]. This slag standardization will effectively eliminate several problems currently associated with the large scale recycling of steel slag.

A maximum limit of 5% volume expansion of the steel slag aggregate has been set as the European standard [2]. In applications where the steel slag is recycled as a bituminous-bound aggregate, as seen in Figure 1, the asphalt binder acts to protect the slag and inhibits the process of hydration and subsequent volume expansion of the free lime and magnesia. However, serious problems may still result if water is able to penetrate through the asphalt-binder and react with the aggregate.

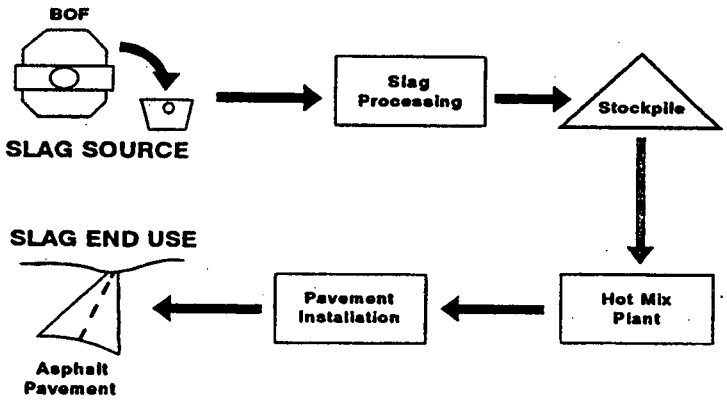

Figure 1. Processing of steel slag as bituminous-bound aggregate for road construction [4]

In Canada steel slags have been used in Ontario as aggregate in hot mix asphalt for nearly two decades and, in 1990, some 488,000 tonnes of slag were recycled in this manner

[4]. However, the Ontario Ministry of Transportation expressed concerns related to steel slag pavement performance, specifically to map cracking, gray veining, "flushing" of asphalt cement to the pavement surface, and lack of quality when compared to natural aggregate mixes. This led, in 1991, to a ban on the use of steel slag aggregate in road construction. Subsequent to this, the Steel Slag Technical Committee was formed in order to resolve these problems associated with the use of steel slag aggregate in hot-mix asphalt. The findings of the Committee were published by Emery and Ferand [4]. The committee concluded that quality control of the steel slag is the key factor in ensuring high grade aggregate for the hot-mix asphalt industry.

The report reasoned that volume expansion of the steel slag must be controlled prior to use in the hot-mix asphalt and that this might be accomplished by altering flux and slag practices at the steel plant. Furthermore, the report suggested that the source separation of metallics from the steel slag and optimized handling practices would be required to prevent contamination of the aggregate. From a steelmaking viewpoint, the changes in operating practices necessary to meet their recommendations are not always feasible due to repercussions on steel quality. In any case free lime and magnesia still represent a serious detriment to volume stability and cannot be totally separated from the slag aggregate. Thus, the moratorium on steel slag usage as an aggregate remains, and no economic alternative has yet been found for large scale recycling.

2.0 LIERATURE SURVEY

2.1 Chemical Composition and Mineralogy of Cements

A comparison of the chemical compositions of different cements and slags is presented in Table I. From this table it is apparent that steel slag, like most metallurgical slags, has a chemical composition similar to that of Portland cement. However, there are significant differences, not only in the overall composition, but in the mineralogical species present. Relative to Portland cement, the main compositional differences in the steel slag are the high iron oxide content, which exists in both the di- and trivalent states, and the presence of substantial free lime. Blast furnace slag has a lime to silica ratio ranging from 1.2 to 2.0, which is considerably less than both steel slag and Portland cement. However, the iron oxide (Fe_2O_3) content of blast furnace slag is very low, approximating that of Portland cement, whereas, the ERZ and high alumina cements have combined iron contents and lime to silica ratios similar to steel slag. It may be noted, however, that the iron oxide present in these alternative cements is predominantly in the form of Fe_2O_3.

Table I - Weight % of Chemical Constituents

Constituent	Portland Cement*	Blast Furnace Slag*	Steel Slag†	High Alumina*	Erz Cement*
CaO	64.1	36-45	35	37.7	64
SiO_2	22	33-42	18	5.3	22
Al_2O_3	5.5	10-16	3.6	38.5	2.8
Fe_2O_3	3.0	0.3-2.0	8.8	12.7	6.2
MgO	1.4	3-12	11.5	0.1	0.9
SO_3	2.1	-	-	0.1	1.8
MnO	-	0.2-1.5	6.5	-	-
FeO	-	-	18	3.9	-

*Lea [4], † Stelco Steel Slag

Ordinary Portland cement, which is the most common type of cement manufactured, is obtained by clinkering a finely ground mixture of limestone, clay, and a source of iron oxide[1]. Clinkering (burning) takes place in large rotary kilns by heating the feed material to a temperature between 1300 and 1500^{o}C, (depending on the make up of the charge), and the clinkering hot product exiting the kiln is then air quenched. The goal of the clinkering process is to reform the four predominant oxides CaO, SiO_2, Al_2O_3 , and Fe_2O_3, through various high temperature reactions, into the cementitious mineral phases: tricalcium silicate $3CaO{\cdot}SiO_2$ (C_3S), dicalcium silicate $2CaO{\cdot}SiO_2$ (C_2S), tricalcium aluminate $3CaO{\cdot}Al_2O_3$ (C_3A), and tetracalcium aluminoferrite $4CaO{\cdot}Al_2O_3{\cdot}Fe_2O_3$ (C_4AF). The distribution of these compounds in the final product depends upon the chemical composition, raw material feed, temperature and time of residence in the cement kiln, and cooling rate [1]. Each of these compounds plays a specific role in the production of a quality cement.

Tricalcium silicate, an ortho-silicate of which several polymorphs exist at varying temperatures, is the main strength contributing component of Portland cement. The high temperature forms of C_3S are cementitious and can be stabilized at room temperature by impurity ions, such as Al^{3+}, Fe^{3+}, and Mg^{2+}, which are present in cement systems [5]. This impure form of C_3S is referred to as alite. Alite is the most important constituent of Portland cement because it controls normal setting and early strength development of Portland cement paste, mortar and concrete [6]. When mixed with water alite reacts to form to form both calcium silicate hydrate (C-S-H) and calcium hydroxide (CH). The C-S-H is a rigid amorphous gel of variable composition, whereas the CH is a crystalline structure of fixed composition [6]. The C-S-H gel is the primary strengthening cementitious compound in a hydrated cement paste.

Dicalcium silicate is also an ortho-silicate with many transformations occurring over a large temperature range. The different polymorphs of C_2S exhibit varying degrees of hydraulicity, some being completely non-hydraulic. The hydraulic form of C_2S, found in

Portland cement, is a monoclinic β-C_2S referred to as belite [5]. It is possible to stabilize the belite phase with the same impurity ions used to stabilize alite. Dicalcium silicate does not exhibit any definite setting time when gauged with water, but develops considerable strength over a period of several days [1]. The products of hydration which result, upon mixing with water, are the same as those formed by the hydration of alite (C-S-H and CH). However, there is a greater proportion of C-S-H produced during the hydration of alite, futhermore the rate of hydration and microstructural developement of alite is 20-times faster than belite [6].

Tricalcium aluminate has an instantaneous set when mixed with water, producing considerable amounts of heat [1]. The hardened product, however, loses strength and begins to crumble when in subsequent contact with water. The strength properties of C_3A in Portland cement still remain unclear. However, Lea [1] has reported evidence suggesting that tricalcium aluminate increases the rate and strength development of C_3S and thus is an important constituent of Portland cement none the less.

The last of the four principle cement compounds, C_4AF, exhibits hydraulic properties similar to that of tricalcium aluminate. The ferrite phase hydrates fairly rapidly and to completion within a few hours of mixing. The ferrite minerals present in Portland cement are actually a series of solid solutions ranging from C_2A-C_2F. C_4AF is the most common ferrite mineral present which is a ternary compound known as brownmillerite. The strength contribution of this pure compound in a cement paste remains uncertain.

When gypsum is added to the cement, which is typically used to control setting of Portland cement, the tricalcium aluminate and ferrite phases hydrate to form ettringite and/or monosulpho-aluminate hydrate [6] These hydrate phases are common in Portland cement pastes and are referred to as the AFt and AFm phases respectively. These sulphate based hydrate phases play an integral role in the overall hydration and strength development of Portland cement. During the hydration of Portland cement all the overlapping chemical reactions between the individual mineral species and water occur sequencially, with all of the

hydration products contributing, at some stage during setting, to the strength of the final product [6].

2.2 Equilibrium Phase Diagrams Relevant to Portland Cement

Although cement manufacturing is not an equilibrium process, considerable insight can be achieved by examining the phase diagrams relevant to Portland cement. The ternary system $CaO\text{-}SiO_2\text{-}Al_2O_3$, seen in Figure 2 [1], is of central importance to cement chemistry. The significant area of this ternary system is the tricalcium silicate phase field bordered by the lime and dicalcium silicate primary fields. The chemical composition of the majority of Portland cements lie in this region, as is indicated in Figure 2. Tricalcium silicate does not form eutectics with lime, tricalcium aluminate, and dicalcium silicate, but rather forms invariant points [1]. This is of considerable interest because tricalcium silicate is the major strength contributing compound in ordinary Portland cement.

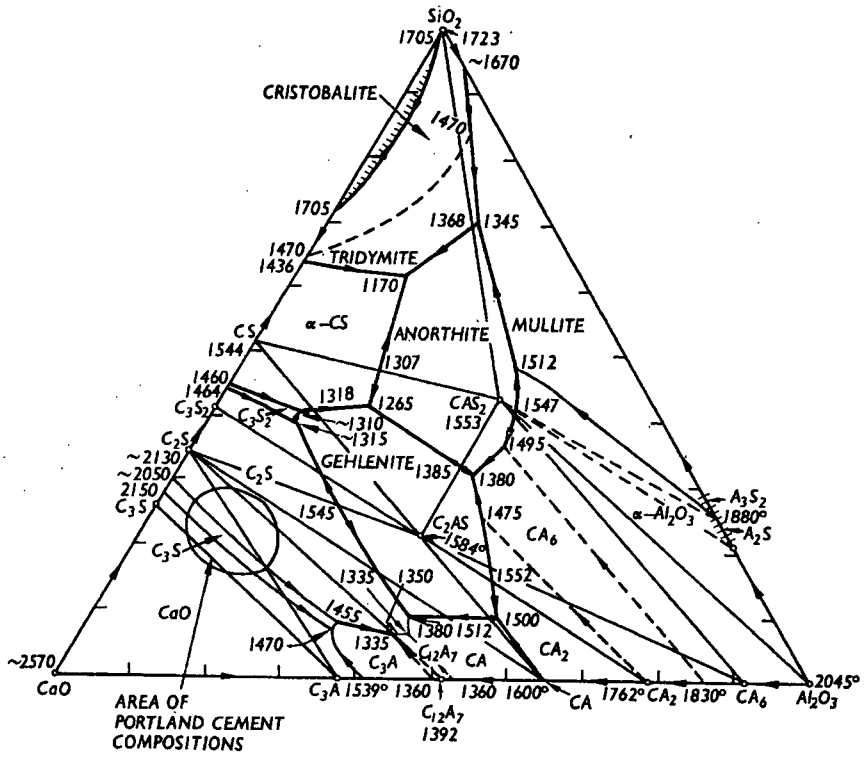

Figure 2. Ternary phase equilibrium system $CaO\text{-}SiO_2\text{-}Al_2O_3$ [1]

Assuming a clinkering temperature of Portland cement at approximately 1500°C, the phase diagram suggests that the lime content of the system plays a significant role during cooling of the ternary system. For example, a cement composition on the high lime side of the C_3S phase field will consist of a liquid and C_3S at this temperature. Upon cooling, the composition of the liquid will move through the tricalcium silicate phase field while C_3S is precipitated out. This will continue until the C_3A boundary is met, at which point it will also begin to separate from the melt and the composition of the liquid will move along the C_3S-C_3A boundary until the invariant point C_3S-C_3A-C_2S at 1455°C is reached. Here C_2S will also separate and the remaining liquid will solidify [1]. By contrast, a mix of lower lime content siting on the C_3S-C_2S boundary will consist of a liquid and both solids C_3S and C_2S at

1500°C. During cooling the liquid composition moves down the C_3S-C_2S boundary while both solids continue to precipitate. At the C_3A boundary all three solids will precipitate from the liquid and crystallization of the remaining liquid will occur [1].

In both cases the final crystallization of the melt takes place outside of the C_3S-C_2S-C_3A triangle. Therefore, the final liquid to crystallize could not alone form the three phase of the triangle due to a lime deficiency in this final liquid. If equilibrium conditions were to exist, the tricalcium silicate precipitate would eventually be redisolved into the melt at the quintuple point to account for the lime deficiency. After a sufficient period of time the final equilibrium products to crystallize from the melt would then be C_2S, C_3A, and $C_{12}A_7$ [1]. However, it should be noted that equilibrium is not acheived during the clinkering process and that the air quench applied to the product effectively freezes the tricalcium silicate present at high temperature.

Two other significant cementitious zones exist within the CaO-SiO_2-Al_2O_3 ternary system, as seen in Figure 3. Both the high alumina and high silica regions have found commercial application, the former as aluminous cements and the latter as blast furnace slag cements. These two cements are considered to be lime deficient relative to Portland cements, which usually tend to have a lime content above 65 %. However, these low lime cements are characterized as low energy slow hardening cements with excellent long term strength.. The slow set is attributable to a decrease in the amount of rapid setting C_3A present. This decrease in tricalcium aluminate is due to the replacement or substitution of Al_2O_3 with Fe_2O_3, which is not included in this ternary system. The ERZ cements which are also considered to be low energy cements, in which Fe_2O_3 has replaced the Al_2O_3 component, exist in the same lime range as Portland cement along the lime silica border of Figure 3.

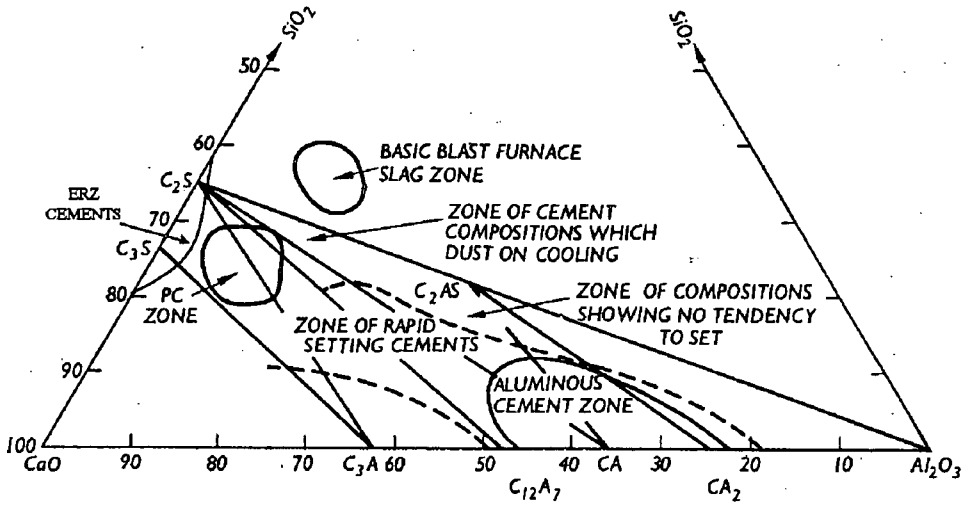

Figure 3. Alternative cementitious zones within the CaO-SiO_2-Al_2O_3 ternary system [1]

The ternary system CaO-Fe_2O_3-Al_2O_3 contains the ternary phase brownmillerite C_4AF, which is the most common ferrite phase in Portland cement. It has been established that the ferrites and aluminoferrites present in Portland cements are of variable composition which is dependent upon bulk composition, temperature, and solid solution composition [7]. Numerous methods have been used to investigate and establish the presence of this range of aluminoferrite solid solutions lying between C_2F and C_2A, as seen in Figure 4 [1]. The actual composition of the aluminoferrite phase found in Portland cements lies between the solid solution range C_6A_2F and C_6AF_2, with a median value relatively close to that of brownmillerite [8]. The substitution of alumina by a matching percentage of Fe_2O_3 raises the potential C_3S content in the clinker due to the fact that proportionally less lime per unit of R_2O_3 is needed in C_4AF than in C_3A [1]. The extra lime is then available to convert more C_2S to C_3S, whereas, the formation of C_6AF_2 instead of C_4AF would essentially have the reverse effect, decreasing the amount of tricalcium silicate.

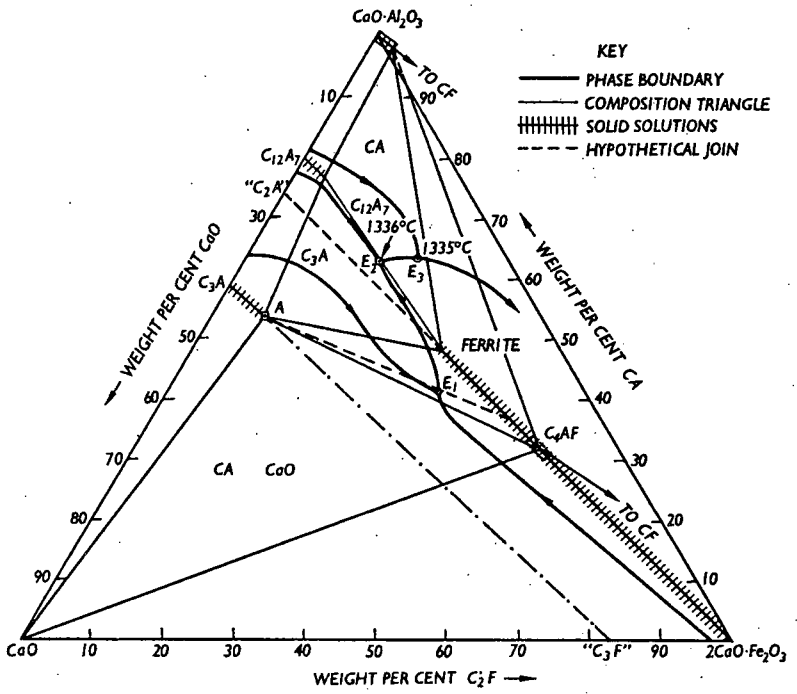

Figure 4. Pseudo ternary system $CaO\text{-}CaO{\cdot}Al_2O_3\text{-}2CaO{\cdot}Fe_2O_3$ [1]

The significant areas of the ternary system $CaO\text{-}Fe_2O_3\text{-}SiO_2$, (Figure 5), are similar to that of the $CaO\text{-}SiO_2\text{-}Al_2O_3$ system. The tricalcium silicate region is once again bordered by lime and dicalcium silicate phase field, the former third phase C_3A is now C_2F. In this system the C_2S phase field is much larger and extends significantly into the region of high iron oxide content. It is clear that no ternary compounds, such as brownmillerite, will form from this system [1]. The Erz cements, located in this ternary system, have similar properties to Portland cement except a lower rate of strength development. This lower rate of strength development is attributable to the decrease in tricalcium aluminate and an increase in the ferrite phase [1]. These cements were found to have a wider field than Portland cement in the $CaO\text{-}Al_2O_3\text{-}SiO_2$ ternary system. The limiting ratio of $SiO_2{:}R_2O_3$ is much lower in Erz cement due to the increase in iron oxide and the low alumina content which is primarily responsible for flash setting [1].

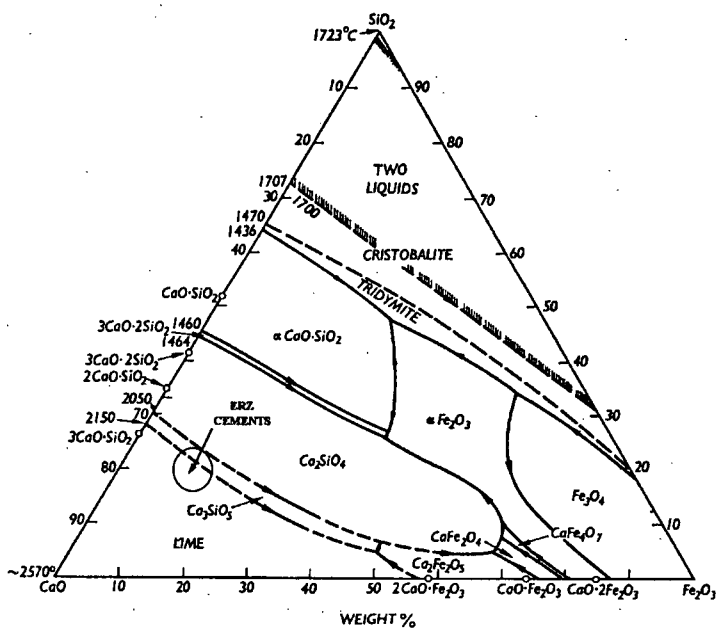

Figure 5. The ternary system $CaO\text{-}Fe_2O_3\text{-}SiO_2$ [1]

By combining the three previously discussed ternary systems it is possible to construct a quaternary system incorporating the four primary oxides as corners of a tetrahedron. Within the $CaO\text{-}Fe_2O_3\text{-}Al_2O_3\text{-}SiO_2$ quaternary system lie the composition of the majority of cements, including Erz, blast furnace, and high alumina. The construction of the pyramid may be seen in Figure 6, with the six sides representing six binary systems. The solid lines of the pyramid lie in the plane of the page, while the dotted ones extend into it. The region of importance, especially to Portland cements, is the smaller quaternary system, within the larger tetrahedron, bounded by $CaO\text{-}C_2S\text{-}C_4AF\text{-}C_{12}A_7$. The composition of modern Portland cements lie within this smaller pseudo quaternary system and their equilibrium cooling paths may be interpreted from it [1].

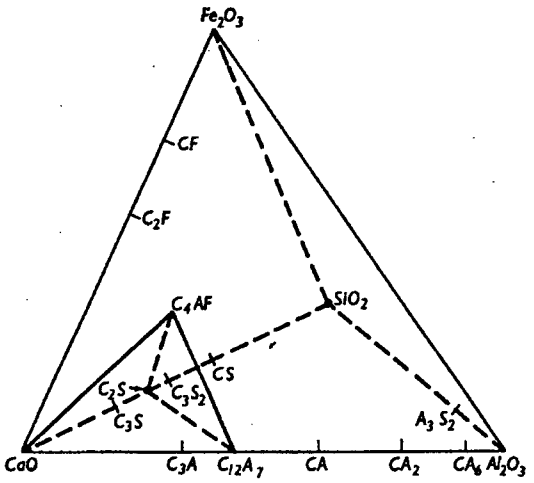

Figure 6. The CaO-Fe_2O_3-Al_2O_3-SiO_2 quaternary system [1]

2.3 Chemical Composition and Mineralogy of Steel Slag

As shown in Table I, steel slags contain all of the oxide components present in the raw materials employed in the manufacturing of cement, as well as being generated at high temperatures. The four key cementitious compounds which characterize Portland cement, might therefore be expected to be present to some degree in solidified steel slags. However, the composition of steel slag is adjusted solely to optimize its refining capability. Furthermore, the cooling rate applied to discarded slag is very slow relative to that of cement clinker, thus it is not suprising that steel slag exhibits poor cementitious properties.

Studies [3,9,10] on cooled steel slag have predicted that the calcium silicate phases are the first to appear, due to their elevated melting point, followed by the ferrites and then wustite and its solid solutions. Although several mineralogical phases are associated with steel slag, the variations in composition and cooling rate of the molten material make it difficult to predict either which mineral phases will form, or the distribution of the various phases which do result. The predominant mineral phases present in solidified steel slag, as determined by Monaco and Wu [3], are shown in Table II.

Table II - Predominant Minerals Associated With Steel Slag [3]

Formula	Name	Synonym	Structure	Melting Point (°C)
3CaO*SiO2	Alite	Tricalcium Silicate	Triclinic	1900
2CaO*SiO2	Belite	Dicalcium Silicate		2130
β-2CaO*SiO2	Larnite		Triclinic	
α-2CaO*SiO2	Bredigite		Monoclinic	
2CaO*Fe2O3	Dicalcium Ferrite	Calcium Ferrite		1430
4CaO*Al2O*Fe2O3	Brown Millerite		Rhombohedral	1410
FeO	Wustite			
MgO	Periclase			2800
CaO	Lime			2570

During cooling of steel slag dicalcium silicate will be the predominat species and is the first solid phase to form in the liquid slag upon cooling [3,9,12,15]. Pure C_2S will undergo a series of complex phase transformation during cooling, from the meta-stable β phase to the stable γ phase, as seen in Figure 7 [11]. This phase transformation is independent of the cooling rate and is accompanied by a volume change, which results in the "falling" or dusting of steel slags. However, the occurence of this phase transformation in steel slags may be inhibited by the presence of impurity ions, which stabilize the β-C_2S lattice structure [3]. C_3S, (alite), will also begin to appear, especially in slags of high basicity, during the early stages of cooling, but will begin to decompose at about 1200°C to C_2S and free lime [10]. This transformation is dependent upon the cooling rate, and may be suppressed if the quench rate is high enough [1,3]. It has been shown that the formation and ratio of C_2S to C_3S is dependent upon the basicity of the slag [12].

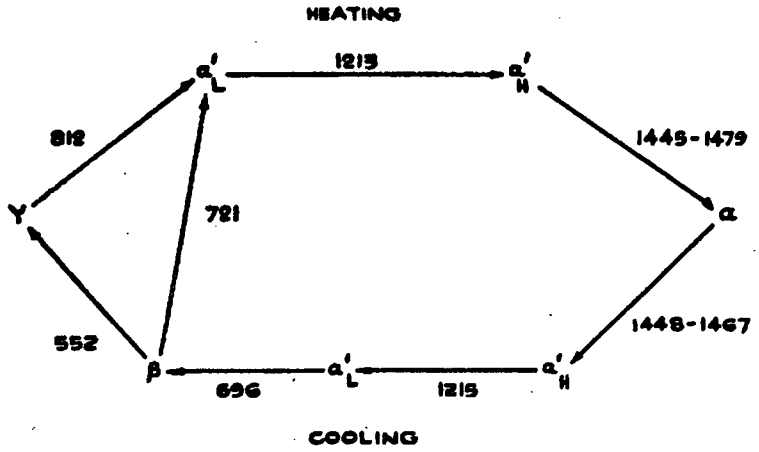

Figure 7. Dicalcium silicate phase transformations [11]

Due to the oxidizing nature of the steelmaking process it is inevitable that certain iron oxides are formed which report to the slag. Monaco and Wu [3] summarized previous work on the presence of iron in steel slags, stating that iron oxide exists in differing valence states as various mineral phases and solid solutions. The most predominat forms of iron oxide in the slag are wustite (FeO) and hematite (Fe_2O_3). CaO, MgO, and MnO are soluble in wustite, forming solid solutions which are stable at room temperature, whereas pure wustite is not. These wustite solid solutions are the most abundant iron oxide phase in slow cooled steel slag. Hematite in the molten slag will combine with lime and alumina to produce a variety of ferritic minerals upon cooling. The calcium ferrites and calcium aluminoferrites can range from C_2F to C_6AF_2 with brownmillerite C_4AF representing the median value [3]. The ferrite phases formed in the cooled steel slag will depend upon the chemical composition and cooling rate [3]. These ferrite phases are always less predominant than wustite.

The valence state of the iron oxide present in the slag will significantly influence the morphology of the final material. Researchers at the Center for Pyrometallurgy [9] have attempted to predict the crystallization path of a typical steel slag using the equilibrium FeO-CaO-SiO_2 ternary system, as seen in Figure 8. This system was chosen because it represents

the primary oxides which occur in steel slag. A slag composition of of 46% wustite, 35.7% lime, and 18.9% silica was chosen based on an average of different slag sources and re-proportioned to eliminate the presence of other oxides. It was assumed from the ternary system in Figure 8 that if a slag of such a compositon, existing within the CaO-FeO-C_2S triangle, were allowed to cool, the final solid phases present in equilibrium would be β-2CaO-SiO_2, wustite and lime. However, it is unlikely that equilibrium conditions ever exist in solidified steel making slags due to the presence of impurities, which will affect the melting temperatures and cooling conditions. The slag usually undergoes an initial quench followed by a slow cool.

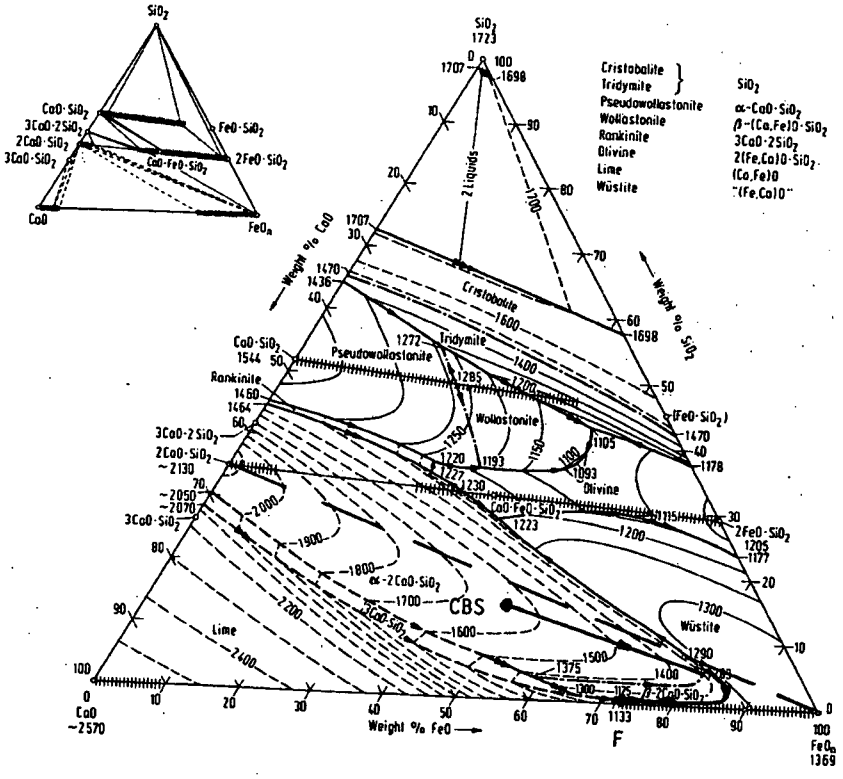

Figure 8. The equilibrium ternary system CaO-FeO-SiO_2 [9]

During subsequent observations on a commercial steel slag, it was determined that wustite had been the first phase to crystallize out of a glassy silicate phase [9]. The glassy phase was hypothesized to have a dicalcium silicate composition. The ternary phase diagram would suggest that with the highest melting point, dicalcium silicate should have been the first phase to crystallize from the melt. This was not the case and might be explained by the formation of a glass during the initial quench of the slag. It has been reported [9] that in high sulfur slags wustite is generally the first crystalline phase, which is unlike high phosphorus slag where dicalcium silicate is the initial crystalline phase. The third most abundant phase in the study [9] was laths or plate-like grains of tricalcium silicate. It was assumed that the initial quench would freeze the tricalcium silicate crystals inhibiting the expected phase transformation.

Both the study by Monaco and Wu [3] and Nelson [9] identified wustite and dicalcium silicate as the predominant phases in steel slags. In contrast to the study by Monaco and Wu [3], which positively identified the calcium aluminoferrite phase brown millerite (C_4AF) as the third most predominant mineral, Nelson [9] tentatively identified this to be the fourth and least predominant mineral in the cooled steel slag and the third phase to be tricalcium silicate. Monaco and Wu [3], however, did not report finding any tricalcium silicate during their research and felt that free lime present in their samples would have hydrated or pulled out during polishing. Both studies reiterated the fact that the presence of tricalcium silicate is dependent on the cooling rate, which suppresses the phase transformation of C_3S to free lime and C_2S. It may be assumed that the differences in the mineral species found in these studies are attributable to the type of commercial slag studied, its initial composition, and the cooling conditions.

2.4 Comparison of Mineral Structures of Steel Slag Relative to Portland Cement

The cementitious properties of steelmaking slag may suffer due to the differences in mineralogy relative to Portland cement. The key to this deficiency is most likely a lack of tricalcium silicate which is the primary strength contributing phase during Portland cement hydration. In addition, wustite solid solutions, which are a predominant mineral phase in steel slag, do not occur to any significant degree in Portland cements. These solid solutions have no inherent cementitious properties and do not combine to form hydraulic minerals during cooling from the melt. Wustite has the ability to take up to 27% calcia into solution [9], thus using up much lime which would be used to combine with silica to form hydraulic tricalcium silicate. In contrast to wustite, hematite will, given suitable processing conditions, form calcium ferrites, calcium aluminoferrites, or go into solution replacing alumina, all of which have hydraulic potential in cementitious systems [7,8,13,14]. The valence state of the iron oxide can have a marked effect on the cementitious properties of the steel slag.

It might be noted that cements with good strength are produced having comparable levels of iron oxide to steel slag. High alumina and Erz cements have high contents of iron oxide, 12-18% and 6-12% respectively, which exists mainly as Fe_2O_3. High alumina cements have reported iron oxide contents as high as 20%, in which calcium aluminoferrites are a predominant mineral species [1]. Erz cements have a considerable amount of Fe_2O_3 with very little alumina present, and a silica/iron oxide ratio of 1.5. These cements show all the physical properties of Portland cement with the exception of a reduced rate of strength development, due to a reduced amount of C_3A and an increase in C_4AF [1]. The higher valence state ferric oxide present in these cements is integral to the formation of strength contributing compounds.

2.5 Steel Slag Cements

Two different approaches exist in the incorporation of steel slag in cement production. The first involves a simple substitution of slag into the raw material feed to the cement kiln by blending with limestone and clay. There is no energy saving as the slag must be clinkered, and no real economic benefit because one inexpensive material is substituted for another. A more attractive approach involves inserting the slag downstream of the clinkering operation by blending with Portland cement clinker, gypsum, and possibly blast furnace slag. These blended cements have a clear economic advantage due to the substantial savings in energy costs which can be realized [15].

Several studies [15,16,17,18] have been performed in which ground steel slag has been blended with a variety of different materials. Sun and Yuan [17] used only steel slag and gypsum to form a cementitious paste. This steel slag cement had low early strength which increased with time. This cement, however, lost stability after steam treatment. Compressive strengths of 49.3 MPa were reported by Wang and Lin [16] for a blended steel slag cement with 60% Portland cement clinker and 5% gypsum. As well Idemetsu [18] reported compressive strengths of 49.2 MPa for samples of 60% steel slag, 33% ground blast furnace slag, 4% gypsum, and 3% calcium chloride as an activator. Montgomery and Wang [15] have made blended cements with strength comparable to that of Portland cement. Mixes of 40.5% steel slag, 40.5% granulated blast furnace slag, 10% Portland cement clinker, and 9% gypsum attained a strength of 34.5 MPa after 28 days. Sun and Yuan [17] have shown that the compressive strength of a mortar made with steel slag, granulated blast furnace slag, and gypsum is dependent on the amount of tricalcium silicate in the steel slag used. When the amount of C_3S is less than 10%, the compressive strength at 28 days is less than 10 MPa. However, when the amount of C_3S is in excess of 40%, all 28 day compressive strength results exceed 30 MPa.

In all these studies ground steel slag was blended "as is" with other cementitious materials to form solidified paste with strengths comparable to ordinary Portland cement. In all cases it is difficult to quantify the strength advantages or disadvantages incurred due to the presence of steel slag. It has been suggested that the excess free lime present in the steel slag would assume the role of activator when blended with blast furnace slag.

2.6 Blast Furnace Slag Cements

Roy and Idorn [19] have reported that slag cements and blended cements containing large percentages of slag are characterized as low heat, slow strength developing cements compared with ordinary Portland cement. The advantages of their use is usually due to their favourable long term strength gain and resistance to aggressive chemical action [19]. The composition of slags potentially suitable for cement manufacture fall into the quaternary system SiO_2-Al_2O_3-MgO-CaO, but may vary greatly in hydraulic properties. This depends upon chemical composition, the presence of constituents other than those of the quaternary system, the amount of crystalline material in the quenched slag, and various other factors [20].

Blast furnace slag is usually poured from the blastfurnace in a molten stream at 1400-1500° C. As the liquid issues from the tap hole in the blastfurnace it encounters a jet of cold air or water which acts to quench the molten slag. This rapid cooling will prevent the crystallzation of the slag, while simultaneously causing the vitreous materials to break up into small glassy granules due to thermal shock [1]. This granulation process essentially freezes the liquid condition of the molten material and settles the latent hydraulicity of the glassy slag [22].

2.7 Glassification of Slags

Glassified slags are essentially undercooled liquids of extremely high viscosity, which inhibits the rearrangement of ions into their crystalline structure [1]. The granulation process rapidly lowers the temperature of the melt, thereby inversely effecting the viscosity and inhibiting the movement of the ionic species to their crystalline lattice positions. The quench freezes the molten liquid rapidly passing through the temperature range in which nucleation and crystallization normally occur. The glassified slag, which under equilibrium cooling conditions would form a crystalline solid, exists in a metastable state. However, for the ions to be able to rearrange themselves into a crystalline structure, the glass would have to be heated until the viscosity had been sufficiently reduced, allowing increased ionic mobility resulting in the subsequent divitrification of the slag.

The glassified slag is considered to have an excess of internal energy attributable to quenching. This metastable state exists because the non-crystalline solid has a greater energy content than that of the parent crystalline phases [21]. The structural arrangement of a metastable non-crystalline solid consists of a three dimensional network similar to that present in crystalline materials. Glass theory suggests that a statistical arrangement of the tetrahedral network does indeed exist; however, the repetition of a strict atomic arrangement of the tetrahedral network is limited, existing only in short range order unlike crystalline structures which are of long range order. For this reason the non-crystalline structure of the glass offers no sharp X-ray pattern, but rather a broad banded amorphous hump.

Schroder [22] stated that in slag melts the oxide components are disproportionately bound into complex ions of differing sizes. The structural arrangement of the ions in glassy systems into coordinate lattices is a consequence of both ionic and covalent bonding forces. In the case of silicate based slags, the central silicon atom Si^{4+} of the tetrahedron, surrounded by four oxygen ions, will influence the valences of adjacent silicon ions through bridging

oxygen links. This forms a spacious lattice which has the ability to incorporate metallic cations due to their coordination trend and following the laws of electroneutrality [22].

The cementitious potential of an amorphous slag is directly attributable to the glass and its ability to hydrate with relative ease [1]. Silicon and aluminum ions are considered to be the primary network-forming ions in slag systems. These ions link together by sharing oxygens in the tetrahedral network. The aluminum ions assume the role of either network-former or modifier and replace Si ions to a limited extent. This substitution in the tetrahedral network increases interionic distances between oxygen ions and cations, thereby opening the structure and enlarging voids to harbour metallic ions, such Ca and Mg.

The decrease in viscosity of the silicate melt with increasing temperature is attributable to the growing number of thermal linkage fractures. Furthermore, an increase in metallic oxides, which foster the coordination trend of the SiO_4^{4-} complex anion, will encourage chemical linkage fractures [22]. As the basicity of the slag melt increases, the viscosity will decrease, thereby improving flow properties of the liquid. This improvement is due to the breakdown of the SiO_4^{4-} tetrahedral network into smaller complex silicate anions as the basic oxide content rises. The relationship between the breakdown of the SiO_4^{4-} tetrahedral open lattice structure and the presence of smaller complex silicate anions is shown in Table III [22].

Table III - Relationship between Basicity and Viscosity [22]

Basicity	Silicate Structure	Relationship O/Si	Viscosity η
Acid	SiO_2	2.0	Higher
↑	$2SiO_2+O^{2-}=Si_2O_5^{2-}$	2.5	↑
	$Si_2O_5^{2-}+O^{2-}=2SiO_3^{2-}$	3.0	
↓	$2SiO_3^{2-}+O^{2-}=Si_2O_7^{6-}$	3.5	↓
Basic	$Si_2O_7^{6-}+O^{2-}=2SiO_4^{4-}$	4.0	Lower

The bonding forces in molten slags, at temperatures between 1500 and 1600^{O}C, which act between cations and anions are broken by thermal and chemical linkage fractures. The thermal fractures are reversible. This indicates that as the slag melt passes into the vitreous state the thermal fissures in the lattice structure begin to close. Therefore, in order to produce a glassy solidified slag with ideal hydraulic properties, it is necessary to cool the melt at a rate faster than the lattice fractures can reform [22]. In this fashion the crystalline lattice cannot form and the liquid structure is frozen into the granulated slag.

In the case of high lime slags the network theory of slag melts begins to yield to the complex ion theory. In this case isolated clusters of disproportionate anions are present and have a greater propensity to crystallize. As the content of base oxides increases, large complex anions begin to form, dividing the tetrahedral network, and are surrounded by cations in the liquid, thereby saturating their free negative charges [22]. Slag melts of this type are considered to be on the limit of glass forming systems and will have a tendency to crystallize if kinetic criteria for glassification are not met by rapid cooling.

The lime to silica ratio is extremely important in granulated slags as it will influence the properties and processing factors of the slag melts. Slags of high silica content are easily cooled to form a predominantly amorphous product, while those of high basicity are more difficult to prevent from crystallizing. Granulated slags of high basicity will generally have a greater hydraulic potential when activated by alkaline additives. The intrinsic potential of the hydration products is directly influenced by the lime concentration of the cementitious paste and this is determined by the activator and the speed at which calcium ions can be freed from voids in the glass network [1].

2.8 Hydration of Blast furnace Slag Cements

It is well known that granulated blast furnace slags are not normally hydraulic at room temperature, but require both activation to initiate hydration and a mechanism for continuing the hydration process. The glassy phase which constitutes the bulk of properly granulated blast furnace slag is thermodynamically metastable with respect to an assemblage of crystalline phases having the same total composition. A large free energy change is consequent upon the formation of hydrated phases, both crystalline and semicrystalline, Figure 9 [19]. Some slag hydration takes place immediately after mixing with water, and a protective layer is formed on the surface of granulated blast furnace slag, which inhibits water penetration to the slag particle and further dissolution of ions from the slag [23]. Numerous species serve as activators and accelerators. Portland cement and the alkalis, gypsum, and $Ca(OH)_2$ act as activators and reactants.

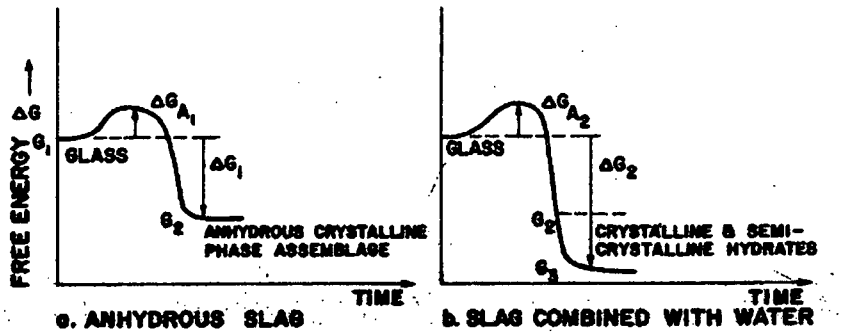

Figure 9. Schematic free energy diagrams for granulated blast furnace slag [19]

Alkaline activators accelerate the dissolution of Si and Al ions by breaking the Si-O and Al-O bonds in the glassy slag structure [1]. This is followed by precipitation of low-solubility calcium silicate, calcium aluminate, and magnesium aluminate due to increased ionic concentration in the liquid phase. At high pH values the dissolution of Al is especially accelerated, which consequently initiates the slag hydration [23].

Roy [23] has stated that the hydration of slag generally requires the breaking of bonds and dissolution of the three-dimensional network structure of the glass. The network contains interlinked SiO_4 and AlO_4 tetrahedra and AlO_6 octahedra which are attacked by the OH^- ion in the high pH environment. Sustaining the hydration of the slag requires a continuous supply of hydroxyl to the slag particle surface. The acitvator will produce an adequate supply to accomplish this goal because the amount of hydroxyl and calcium ions produced from the slag alone are not sufficient [23]. Another requirement which also assists in slag hydration is the developement of an appropriate hydrate structure on the surface of the slag [23]. The formation of such a structure is determined by several physical conditions as well as the OH^- ion concentration in the cement paste.

A model for the long-term hydration of blast furnace slag cements was developed by Roy and Idorn [19], as seen in Figure 10. During the long-term hydration of blast furnace slag cement there is a retention in the cement C-S-H phases of both calcium hydroxide,

released from residual Portland cement, and of residual alkalis from the slag fraction [19]. A system has been formed which has the continuous ability to increase its amount of C-S-H, and to attain added homogeneity and a fine dense microstructure by consumption of the crystalline Ca(OH) released by the Portland cement fraction in the course of slow, authigenic hydration [19]. The hydration of slag cement therefore continues during the performance stages of concrete and concurrently retains alkalis and calcium hydroxide, all the while contributing to increase the strength, density, and chemical resistance [19].

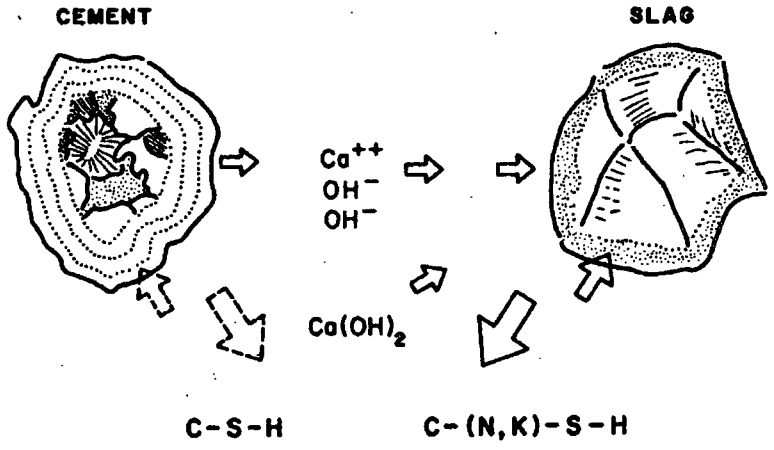

Figure 10. Long term hydration of blast furnace slag [19]

3.0 SCOPE & OBJECTIVES

The overall objective of this project is to determine the processing conditions by which the hydraulic nature of steelmaking slag can be improved to a level which allows blending with conventional Portland cement clinker. Based on the current Canadian production rates of both slag and cement, a modest slag to clinker ratio of 1:10 would allow full recycling of the steelmaking by-product. The benefit to the steel industry is the conversion of a waste product, (and environmental liability), into a saleable, value added commodity. For the cement industry the benefits include lower energy and raw material costs and a substantial reduction of CO_2 emissions. All the benefits accrued by the cement manufacturer are attributable to a lower raw material throughput in the clinkering kiln, per tonne of cement product.

The desired improvement in a slag's cementitious properties might be achieved by the addition of certain oxides, primarily CaO and SiO_2, to the liquid slag, in order to duplicate the basic composition of Portland cement. This oxide addition would then be followed by controlled cooling in order to emulate the crystalline and phase structures present in Portland cement. This approach was not considered because the liquidus temperature of the adjusted slag is sufficiently elevated that substantial additional energy would be required to fully dissolve the oxide addition. Based on information derived from the literature, it was decided to attempt to achieve the desired results through minor adjustments in liquid slag chemistry. The principle adjustment would be the oxidation of FeO to Fe_2O_3, followed by rapid cooling in order to obtain a predominantly amorphous structure containing the principle phase of Portland cement.

An experimental program was, therefore, carried out involving the preparation of several liquid slags from laboratory grade materials, (synthetic slags), as well as Stelco BOF slag. One of the variables included in synthetic slag composition was the oxidation state of

the iron component. These liquid slags were subjected to rapid quench cooling in water or slow cooling in air. The resulting products were then analyzed by XRD and SEM, and their mineralogical structure compared to that of Portland cement. The solidified slags were ground and blended with Portland cement at up to 40% by weight. These blended cements were then hydrated in order to determine compressive strengths of the cement paste at various intervals, up to a 35 day hydration period.

4.0 EXPERIMENTAL PROGRAM

4.1 Experimental Procedure for Sample Preparation

The purpose of the experimental work was to determine the influence of chemical composition (in particular the lime to silica ratio), the valence state of the iron, and cooling rate on the final microstructure and mineral formation in the cooled slags. The study focused on three synthetic slags blended from laboratory grade powders and one commercial BOF steelmaking slag. The overall compositions of these four slags are shown in Table IV. Synthetic blends were used in order to eliminate the compositional variability and extraneous impurities associated with commercial slags produced by different steel manufacturers. It is well known that a considerable degree of variability exists in commercial slags and this variability may be of some consequence in making a cementitious material. This study, however, concentrated on the valence state of iron and composition of the steel slag. For this reason it was decided that synthetic blends of known compositions would be used to determine the formation of cementitious minerals from pure oxides, thereby serving as a standard for commercial tests.

Table IV - Steel Slag Compositions (Weight %)

Constituent	SS1	SS2	SS3	Stelco Steel Slag
CaO	38	48	48	34.9
Fe_2O_3	29	22	3	25.8
SiO_2	15	18	18	17.6
MgO	6.5	12	12	11.6
Al_2O_3	5	-	-	3.6
MnO	5	-	-	6.5
TiO_2	1	-	-	-
P_2O_5	0.5	-	-	-
Fe	-	-	19	n/a

The composition of the first synthetic steel slag (SS1) was based on the average of several commercial slags, with a lime to silica ratio of approximately 2.5 and a ferric oxide content of 29%. This mix, (as in the other synthetic slags used), was prepared from pure oxide powders in order to minimize the presence of unknown impurities found in commercial slags. The iron present in the mix was in the form of hematite (Fe_2O_3), whereas the iron present in industrial slag, (Table I), is usually a mix of wustite, its solid solutions, and ferrite minerals. The liquidus temperature of this blend was determined to be approximately 1500°C.

A second synthetic mix, SS2, consisting only of the most predominant oxides found in steelmaking slag was also utilized. The composition of this second mix was selected to eliminate the extraneous affects of the minor elements on the XRD and SEM analyses, and focus on the main minerals formed from a melt. At a lime to silica ration of 2.66, this mix, (SS2), borders on the high lime side of the $CaO-C_3S$ phase boundary of the $CaO-SiO_2-Fe_2O_3$ system, which is typical of many commercial steel slags. The high lime:silica ratio was selected to promote the formation of tricalcium silicate, with the possibility of free lime existing in the final product. Although the high ratio of lime:silica skirts the O:Si limit of glass forming systems, it was theorized that by quenching and using trivalent iron a predominantly amorphous material could be produced by granulation.

In the third synthetic blend, SS3, elemental iron was added and then oxidized at 900°C in an attempt to form higher oxides of iron. Whether or not the iron was completely oxidized to FeO or Fe_2O_3 was not considered to be critical. The purpose of the test was to confirm that at least some of the iron could be raised to a higher valence state prior to melting, thereby initiating the formation of ferrite minerals.

In addition to the synthetic blends, a commercial slag was included to represent a typical slag produced from an integrated steel mill. The commercial BOF slag was crushed and separated magnetically to remove any large inclusions of iron. The material was then milled and magnetically separated for a second time to form a powder. This particular commercial slag has a high manganese oxide content, attributable to the iron ore used by

Stelco. The iron oxide in this slag is predominantly in the form of wustite with magnesium, calcium, or manganese in solid solution.

Crucibles charged with powdered slag at room temperature, were introduced into the hot chamber of the furnace at 1510° C. The Leco furnace was heated by four resistance Super Kanthal elements. Once the charged crucibles had been secured in the furnace chamber, at 1510°C, they were heated in air for 15 minutes. Once the slags were molten the crucible was removed from the furnace and either allowed to sit and air cool, or the molten slag was poured into a water bath of running water at approximately 7°C. The granulated slag was then collected and dried. Part of the hardened slag samples were set aside for microscopic analysis while the remainder of the material was ground into powder for x-ray diffraction examination and hydration testing.

Due to the corrosive nature of the slags and their differing basicities, a certain amount of difficulty was experienced in selecting an adequate crucible. In most steelmaking BOF operations the refractory of choice is magnesia. Several tests were carried out in porous 300cc industrial grade magnesia crucibles. These crucibles failed due to slag infiltration as the molten liquid entered the crucible wall and caused it to sag. Small dense laboratory grade crucibles made from high purity alumina proved to be the most robust in terms of chemical attack and thermal shock resistance. The only draw back was that a small amount of the alumina crucible was dissolved into each melt, increasing the weight percent of alumina in the final material by approximately 3%, which is a compositional value similar to many steelmaking slags. These small, (100 cc), alumina crucibles were used for the majority of the slag melts with limited success.

Larger high grade, dense, 300cc magnesia crucibles were procured to simulate the refractory used in BOF operations. These magnesia crucibles, however, could not handle the thermal stresses produced when entering the furnace at 1500° C, and then subsequently being exposed to air at room temperature, after the 15 minute heating cycle. Therefore, a composite crucible setup, shown in Figure 11, was developed consisting of an outer silicon-carbide

silicon-nitride bonded Crystalon crucible holding a dense high grade magnesia crucible. The annular space between the two crucibles was packed with alumina powder. The composite crucibles exhibited satisfactory thermal shock resistance for the test work, being able to withstand the thermal cycling involved during melting and quenching. Although the Crystalon crucibles exhibited good resistance to thermal shock they could not directly contact the charge due to their carbon content, which acted to reduce the iron oxides at elevated temperatures. Both alumina crucibles and magnesia composite crucibles were used for the Stelco slag melts in order to determine the extent and effect of alumina and magnesia dissolution into the melt.

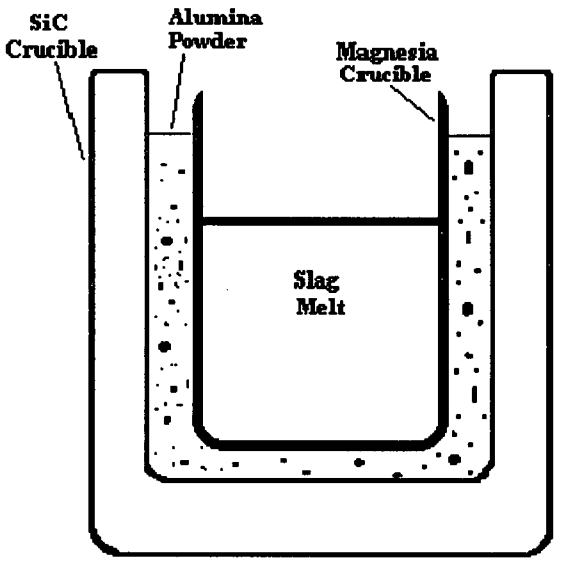

Figure 11. Composite crucible setup

For microscopic examination, samples were mounted and polished to a 1 micron grit. These specimens were then carbon coated and analyzed using SEM and EDX in order to determine the microstructure and composition of differing phases. The X-ray diffraction tests on the powder samples were conducted on a computerized Rigaku Rotating Anode X-ray diffractometer, which is designed for assessment of thin films and powders The peaks from

the resulting diffraction spectra were identified and matched with the JPCDS index to determine possible mineral phases present. The combined results from these tests were used to establish the mineral structures of the slow cooled and quenched products.

4.2 Experimental Procedure for Hydration and Strength Tests

The hydration potential of the different oxidized and granulated slags was investigated by preparing cylindrical specimens from cement pastes and subsequently testing their compressive strengths at progressive ages. Three different oxidized and granulated slags were subjected to hydration testing: synthetic slag SS2 melted in an alumina crucible, Stelco slag from the alumina crucibles, and Stelco slag from the composite magnesia crucible. The slag produced by the granulation after oxidation route was chosen for the hydration tests over the slow cooled slag. Even though the slow cooled slags had improved cementitious potential compared to the untreated slag, they were not included in the hydration testing because they were extremely hard and difficult to grind. In a commercial process this would result in higher energy costs when compared to the quenched slag, where communition is essentially induced by thermal shock. Furthermore, the excellent long term strength and chemical resistance of blast furnace slag cements has been shown to be largely attributable to the rapid quenching process [19,22,23].

In each instance approximately 500 grams was ground in a ceramic mill and sized, according to ASTM method C 184 - 90 [25], to minus 150 mesh. Blends of various compositions, as seen in Table V, were prepared in a rolling mill to ensure proper mixing. In the case of each blend, A through E, three steel slags, (synthetic slag SS2 melted in the alumina crucible, Stelco slag from the alumina crucibles, and Stelco slag from the composite magnesia crucible), were used for the steel slag addition. Therefore, by using three different steel slags, three different lots of each lettered blend, (A-1, A-2, A-3, B-1, B-2...) were

produced. The various blends of Portland cement, steel slag, ground granulated blast furnace slag (GGBFS), and gypsum were then mixed with water, 22% by weight, to form cement pastes. Cylindrical compressive specimens, 12mm diameter x 12mm high, were formed from the cement paste according to a technique used by Meyer referred to in Coale *et al* [20]. The size of the compressive test specimen used in the ASTM standard C 109 - 93 [25] was not practical due to the large amount of material required to produce such test pieces. The cylindrical samples were kept moist until they had set, at which point they were removed from the molds and cured in water until the time of testing.

Table V - Composition of Cement Pastes

Blends	A	B	C	D	E
Cement* (%)	90	80	45	40	10
Steel Slag[1,2,3] (%)	10	20	45	25	40
GGBFS (%)			10	25	40
Gypsum (%)				10	10

* Type 10 Tilbury Portland Cement, 1-Stelco MgO crucible, 2-Stelco Al_2O_3 crucible, 3-Synth. Slag

The different blends were chosen to determine the effect of slag addition on the compressive strength of Portland cement paste. Gypsum was also added to some mixes to activate any glassified slag and enhance the hydration process. Because Montgomery and Wang [15] suggested that blends of blast furnace slag and steel slag would benefit from a symbiotic effect between the free lime in the steel slag and the GGBFS; blends of both 25% and 40% GGBFS were made up (as seen in Table V). Cylindrical compression samples for each mix were tested at each hydration period of: 1 day, 7 day, 14 day, and 35 day. The

compression samples were placed in an Instron mechanical testing machine and loaded until failure.

5.0 RESULTS

5.1 Mineralogical Observations

A standard method of identifying mineral and phase structures is x-ray diffraction (XRD) which, when combined with electron microscopy, allows for the examination of the polycomponent mineral systems associated with cements and slags. The corroboration of these analytical methods provides a method for the identification of the crystalline and amorphous phases found within the quenched and slow cooled slags. It is of fundamental interest to compare the x-ray diffraction trace of a steel slag to that of Portland cement. To this end, an X-ray diffraction pattern for Tilbury Type 10 Portland cement, ranging from 10^{o} to 70^{o} 2θ, is depicted in Figure 12. This XRD trace is typical of commercial Portland cement clinkers.

It may be noted that the peaks of the main mineral phases (alite, belite,C_3A, and the ferrite phase) are concentrated between the 2θ angles of 29^{o} and 35^{o}. This region is expanded in Figure 13. Quantitative x-ray diffraction analysis (QXDA), used to determine the actual amount of each mineral composition, depends on the intensity of a diffracted line, which in turn, is directly related to the crystalline phase producing it [5]. Unfortunately, in the case of the complex diffraction pattern produced by a cement clinker, several factors influence the intensity-quantity relationship so that significant error is associated with a quantitative analysis. The main problem associated with QXRDA of cement clinker is the overlapping of differing peaks.

For example, Figure 13 exhibits significant peak overlap of the calcium aluminate and ferrite phases between the 2θ angles of 33^{o} and 34.5^{o}. Furthermore, the calcium silicate peaks, alite and belite, have overlapping strong lines which translate into difficulties in determining the contribution of each component mineral. These difficulties notwithstanding,

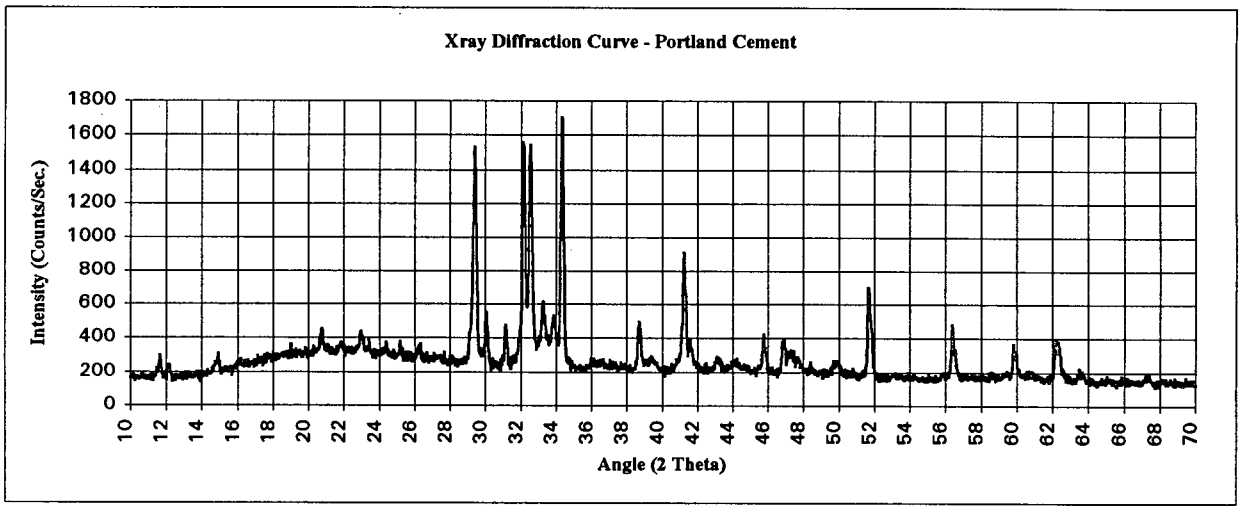

Figure 12. Typical x-ray diffraction pattern for Portland Cement (Tilbury type 10)

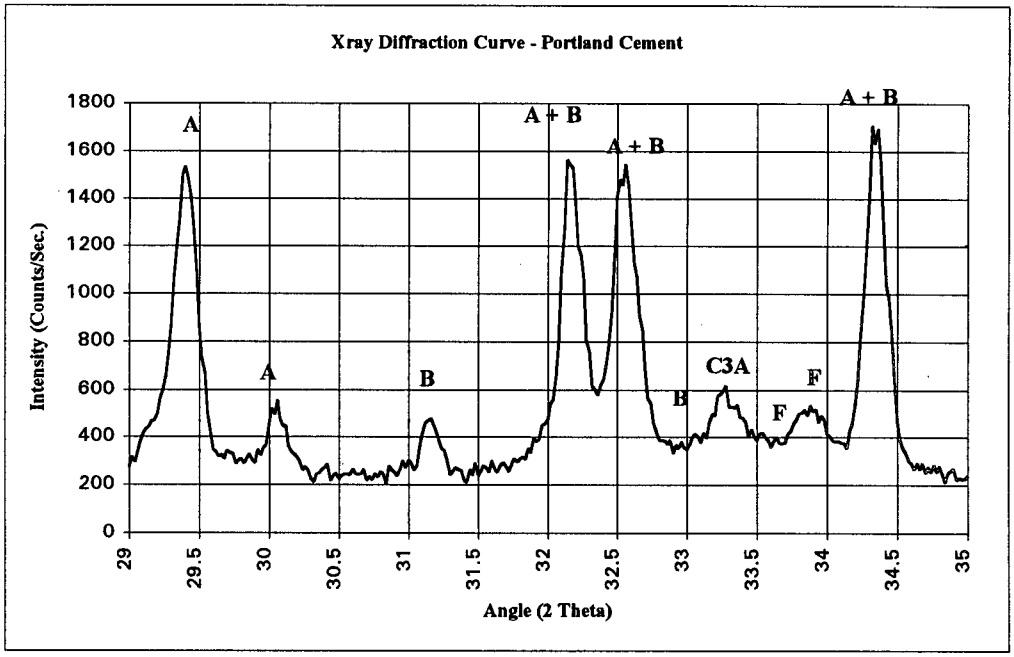

Figure 13. Detail of the x-ray diffraction pattern of the predominant mineral phases in Portland cement: A - alite, B - belite, F - ferrite phase

the quantification of the differing phases and their contribution to the intensity of their respective peaks in Portland cement clinkers has been studied extensively. The alumina and ferrite peaks will shift and change in intensity depending upon the A:F ratio of the clinker. As the iron oxide content in the clinker increases the ferrite phase peak also intensifies, thereby resulting in a shift of intensity from the tricalcium aluminate peaks to the ferrite phase. These effects are shown in Figure 14, for four different C:A:F ratios, ranging from 3C:A to 6C:2A:F.

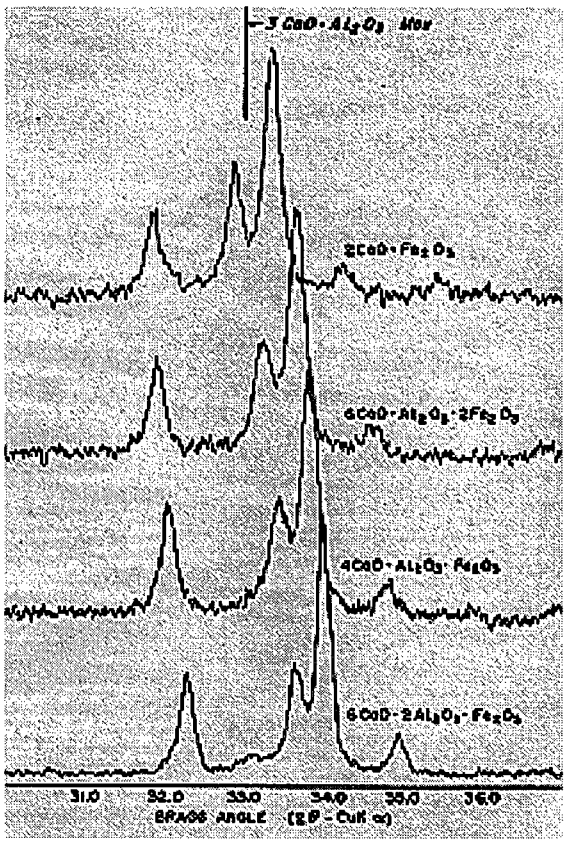

Figure 14. X-ray diffraction patterns of four calcium alumino-ferrites [8].

5.1.1 XRD, EDX, and SEM Analyses of the Synthetic Mixes

The synthetic slags prepared during the course of the work were also subjected to XRD analysis and the results were compared to the Portland cement data. The XRD traces of the slow cooled and quenched samples of the synthetic mixes are shown in Figures 15-17. As might be expected, the x-ray curves of the slow cooled samples have several distinct peaks resulting from a strongly crystalline structure. However, the line broadening of the peaks and the gradual slope at the beginning of each trace suggest that amorphous material is present. The x-ray patterns of the quenched samples are representative of glassy materials, possessing a "hump" between the 2θ angles of approximately 26° and 36°. This "amorphous hump" is characteristic of glassy materials and a technique has been developed which uses the area under the hump to quantify the crystalinity in such a material [26]. XRD traces of materials with varying glass contents, which had been quantified using the "amorphous hump technique", were compared to the XRD traces of the quenched slags to qualitatively estimate the amount of amorphous material.

The purpose of quenching the synthetic slags was to produce an amorphous material simulating the granulation process. The SEM analyses of the individual quenched samples SS1, SS2, and SS3, Figures 18-20 respectively, disclose a relatively glassy surface with substantial macrocracking for all three materials. The cracking was induced by the large thermal stresses encountered during the granulation quench. In general the surface structure of the samples was found to be amorphous and revealed no distinct continuous features. Low magnification EDX analysis of the surface of each sample indicated the amorphous material to be of approximately the same composition of the initial mix. High magnification (2000X) "spot" EDX analysis performed on the samples confirmed the presence of a homogeneous composition of all known elements. However, the quenched specimens did exhibit a few regions of crystallinity amid the amorphous structure, Figures 21-22, which, under EDX analysis, were found to be crystalline domains of calcium silicates (C_3S, C_2S).

These results are in general agreement with Lea [4] who reported that cements, of similar compositions, which had been quenched from a melt at 1450°C, formed C_3S, C_2S, and a glass containing alumina and ferric oxide. The presence of calcium silicates in the glassy material should be expected as the CaO-SiO_2-Fe_2O_3 phase diagram indicates that they would be the first phase to nucleate and crystallize from the melt. This, coupled with the high melting points of C_2S and C_3S, will result in the nucleation and grain growth such as that in Figure 23. The high ratio of lime to silica in the starting material is too basic to produce a completely glassy material [22]. The formation of orthosilicate ions in the slag melt is to be expected, due to the relatively basic O:Si ratio in the melt, resulting in the formation of crystalline calcium silicates upon cooling. Another crystalline structure found in the predominantly amorphous solid was periclase, and was detected using a back scattering technique, which identified the light magnesium oxide in the heavier amorphous material, Figure 24. It is likely that the magnesia formed clumps during mixing and did not have time to completely dissolve into the melt. Undissolved periclase is often found in commercial slag systems as bits of refractory are taken up into the melt.

In contrast to the amorphous structure of the quenched samples of synthetic slags, the slow cooled samples exhibited strong crystallinity under XRD and EDX examination. Thus, the XRD pattern in Figure 15(b) of the slow cooled mix SS1, has several peaks associated with the different crystalline phases. The peaks of particular relevance for hydraulicity are those peaks between the 2θ angles of approximately 29° and 35°. Recalling Figure 13, Portland cement has peaks attributable to the the four major minerals in this region [3,7,8]. Figures 13 and 15(b) indicate that although both tri- and dicalcium silicate are present in the SS1 material, the absence of a strong tricalcium silicate peak 29.4° suggests a deficiency. A search/match of the peaks file with the JCPDS index confirmed the existence of both alite and belite. It is a diffuse rendering of the peaks between the 2θ angles of 28° and 38° which produces the distinctive "amorphous hump" in the corresponding quenched XRD pattern of Figure 15(a).

As the size of the crystal grains decrease and the amount of amorphous material increases, the diffracted peaks become less intense and wider. The size of crystallites can be measured as a function of the half width of the x-ray peak. As the crystallites decrease in size the resultant increase in peak width is known as line broadening [27]. The size of the crystallite has an inverse affect on the width of its associated defracted peak. Eventually, at an extremely small size, the crystallite will consist only of atoms in short range order, thereby producing the same diffraction pattern as a glass. This is the case in the quenched samples, where the extremely small regions of calcium silicate crystallites, Figures 21-22, produced an amorphous hump in the diffraction traces.

A series of x-ray curves for three different quench rates for the mix SS3 depict the influence of cooling on glass content in the slag, as seen in Figure 25(a-c). The amorphous hump method can quantify the amount of glassy material by determining the area of the hump present in Figure 25(a) and (b) [26]. The hump in Figure 25(a) has one distinct peak evolving from the amorphous hump at 33^{o} 2θ. This hump begins to disappear and broad peaks begin to form, 16(b), as the cooling rate is reduced. Eventually at low quench rates no hump is present, and the most distinct and intense peak still occurrs at 33^{o} 2θ. The broadening of this peak, as the cooling rate increases, is a function of the size of the calcium silicate crystals present in the material. The high quench rate could not prevent calcium silicates from nucleating. However, it did inhibit their growth producing very fine crystals with short range order.

The presence of calcium ferrites and calcium alumino-ferrites in the mix SS1 was also confirmed by the search with the JCPDS index, and this was expected due to the high composition of calcium in the initial mix. The equilibrium ternary phase diagrams indicate that lime would combine first with silica to produce alite and belite, and the remaining lime would then be free to form tricalcium aluinate and brownmillerite [1]. The search also suggested the presence of magnesio ferrites ($MgFe_2O_4$, $MgAlFeO_4$). The strong peaks of these magnesio-ferrites are apparent at the 2θ angles of approximately 35.5^{o}, 57.2^{o}, and 63^{o}.

These peaks will shift depending upon the amount of aluminum present in the magnesio-ferrites.

The strong magnesio-ferrite peak, in the slow cooled SS1 pattern, at 35.5° 2θ and the intensity of the calcium silicate peaks is considerably less than in Figures 16(b) and 17(b). The magnesio-ferrite peak at 35.5° 2θ was able to form due to the lower CaO to SiO_2 ratio of mix SS1. The lime in the system initially combined with silica to produce alite and belite, and then combined with iron oxide to form a calcium alumino-ferrite phase. Once the free lime is depleted in the system, the iron oxide is free to form magnesio-ferrite rather than a brownmillerite phase. The lower lime to silica ratio in this synthetic (S.S.1) mix is also responsible for the decreased intensity in the calcium silicate peaks.

In the SEM micrograph of slow cooled SS1, Figure 26, irregular flake-like grains are evident, and spread concentricly from a central "sun burst" into a light gray matrix. The dark gray flake-like grains are calcium silicates with varying ratios of CaO to SiO_2, ranging from 1:1 to 3:1. The equilibrium phase diagram suggests that in a melt with the C:S ratio in the mix SS1, all the silica would initially form alite. Alite would then decompose forming belite and lime as the temperature drops. However, the non-equilibrium cooling conditions dictate that some of the alite was stabilized due to rapid cooling. The gray matrix in the figure consists of light and dark sections. The light regions are an amorphous mix of all the elements except silica, whereas the darker gray areas in the matrix are calcium ferrites. It is common to produce a calcium alumino-ferrite phase when the ferric oxide content is high in the slag melt. This phase varies from pure C_2A to C_2F, and forms a phase with a composition approximated by brownmillerite. Even though the samples were slow cooled , they were subjected to a room temperature air quench from 1500°C, which would freeze some of the melt and form the light grey amorphous matrix in Figure 26. It seems probable that this glassy region would be devoid of silica as all of it has combined with lime to form the calcium silicates.

In Figures 16(b) and 17(b) the diffraction curves for the two slow cooled synthetic mixes SS2 and SS3 are similar. A search/match of both curves indicated the presence of periclase and a small amount of free lime, in addition to those structures found in the synthetic mix SS1. The presence of free lime could not be confirmed using microscopic examination, due to hydration during polishing. However, thermodynamics and the XRD data corroborate its existence in the solidified material. As expected, the diffraction information also indicated the presence of calcium silicates. Furthermore, the presence of alumino-ferrites and magnesio-ferrites was detected.

Figure 27 is a micrograph of slow cooled SS2 with large circular calcium silicate grains in a light gray matrix. The calcium silicate microstructure is considerably more defined and regular than in case of slow cooled SS1 (Figure 26). The EDX indicated the grains to be either C_3S or C_2S with the tricalcium silicate as the predominant phase. The EDX also showed the matrix to be mainly calcium alumino-ferrite phase with the other elements present in solution. The dark spots in the matrix were identified by the EDX as periclase, which is consistent with the findings from the backscattered photographs (Figure 25) of the corresponding quenched samples. An EDX scan of the surface of the sample indicated that the alumina content had indeed increased, due to dissolution of the crucible. This result confirms the possible existence of calcium alumino-ferrites, which had not been anticipated due to the absence of alumina in the starting material. The sample of slow cooled SS3 "dusted" during cooling. As a result of dusting, which is typically attributable to a phase change in C_2S, an SEM analysis was not possible; however, the x-ray search/match attested to the presence of large amounts of C_2S.

It is difficult to predict which phase of C_2S formed in the slow cooled slag. It may be assumed that the beta phase had formed and was stabilized by the presence of impurity ions (Fe^{2+}, Al^{3+}) and the cooling rate. The presence of the gamma phase was only detected in the sample SS3 which dusted upon cooling. The C_2S in the slag is customarily present as the β polymorph, which infrequently transforms to the γ phase when cooled. There is a volume

change associated with this phase shift. This volume expansion, which can occur in Portland cements, is known as "falling" or "dusting", and produces a fine powder [8]. It should also be noted that the gamma phase of dicalcium silicate does not possess the same hydraulic properties as the beta phase; therefore, it is desirable to suppress this transformation [4].

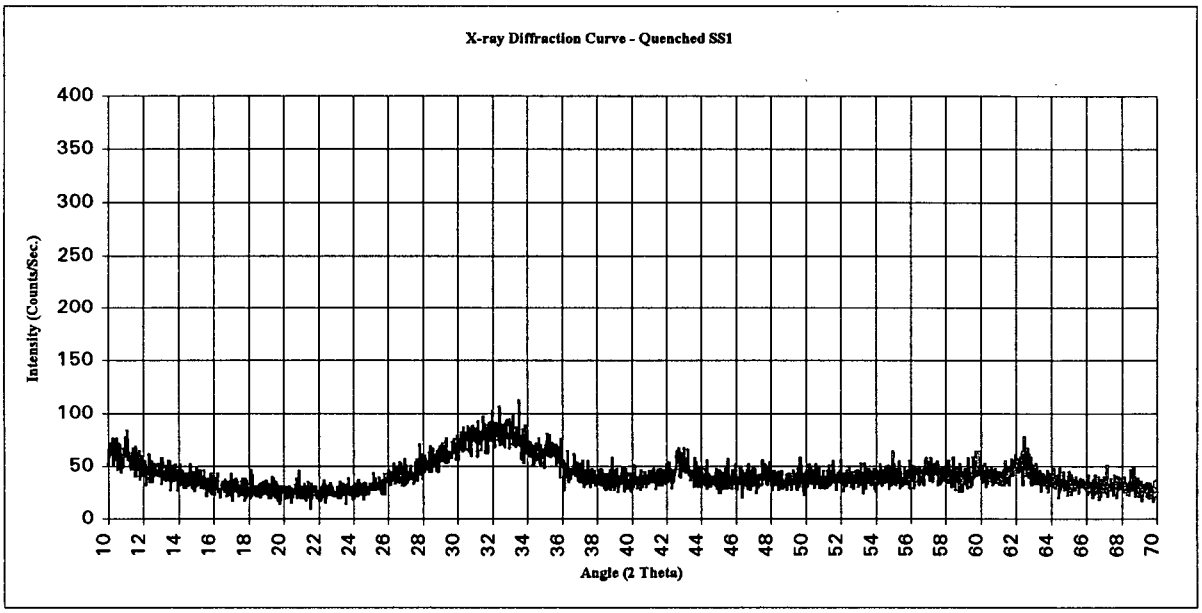

(a)

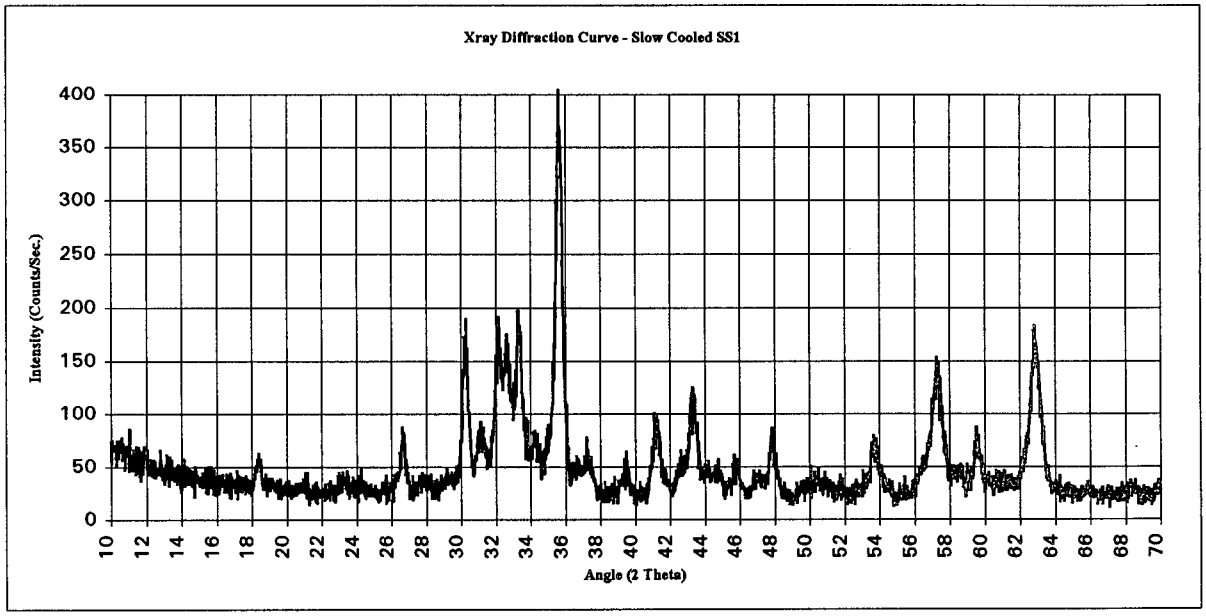

(b)

Figure 15. X-ray diffraction pattern - (a) queched and (b) slow cooled SS1

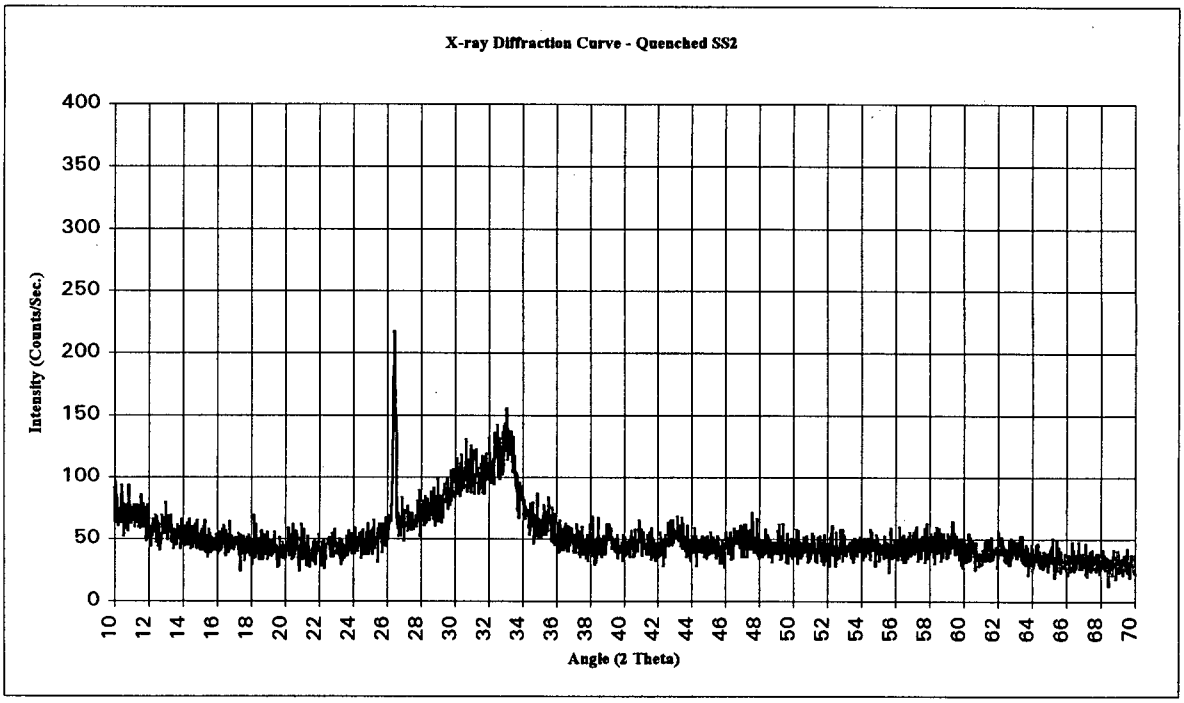

(a)

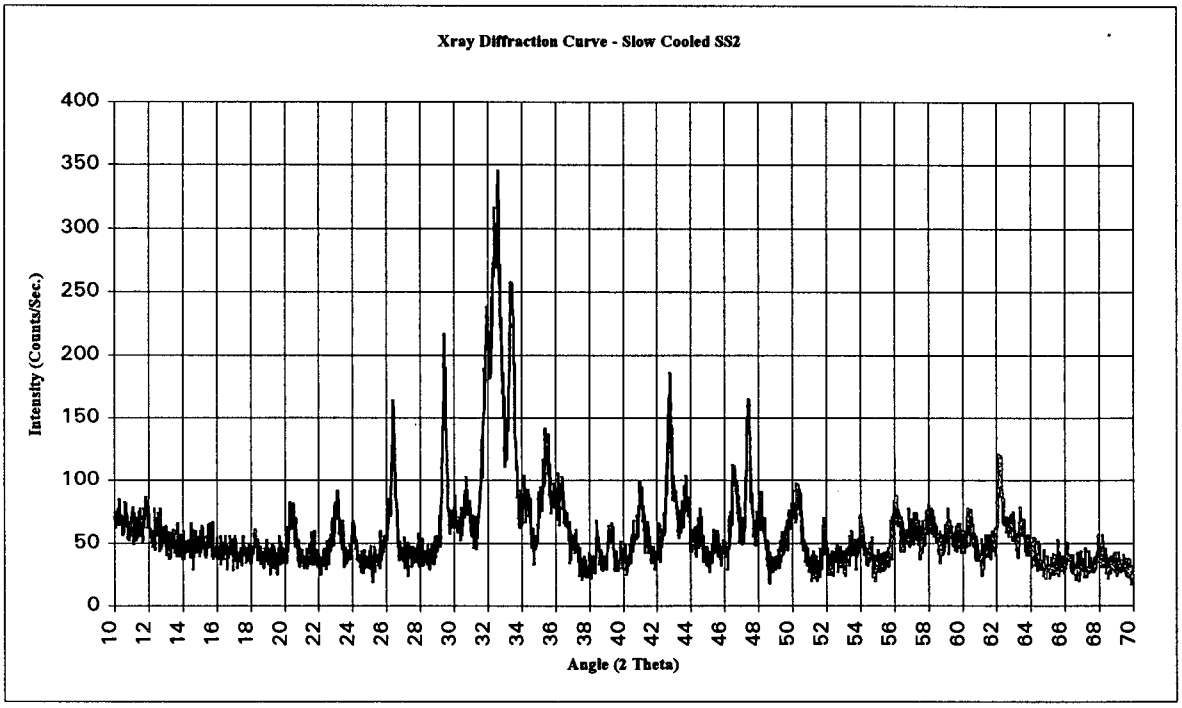

(b)

Figure 16. X-ray diffraction pattern - (a) queched and (b) slow cooled SS2

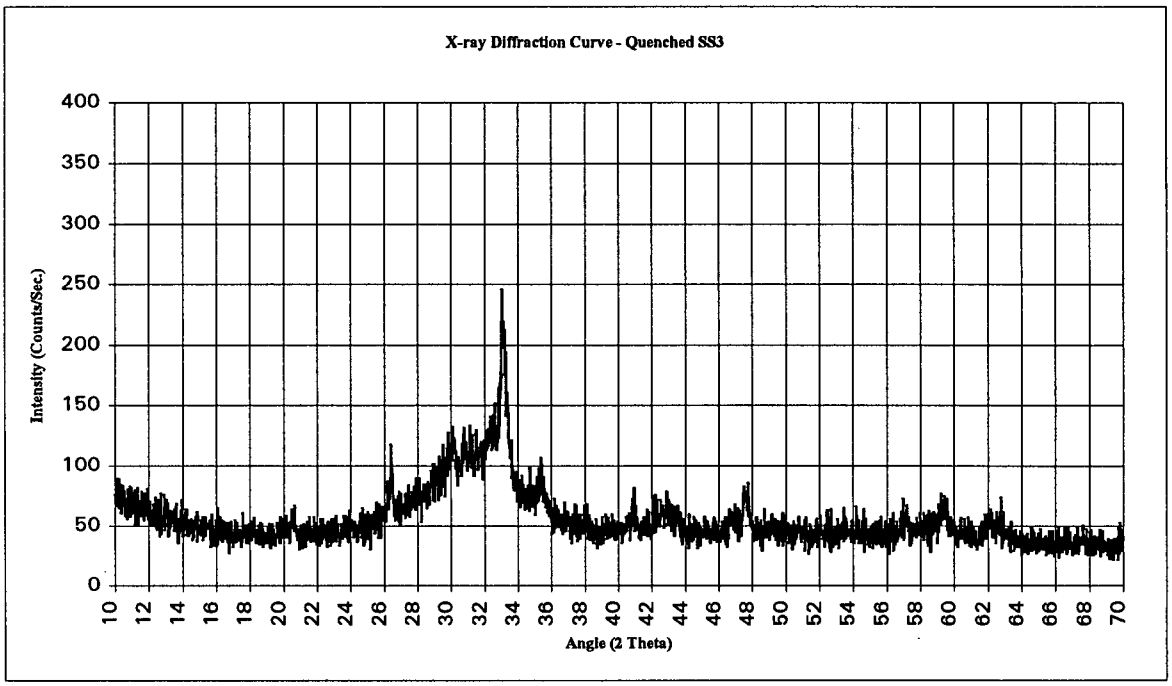

(a)

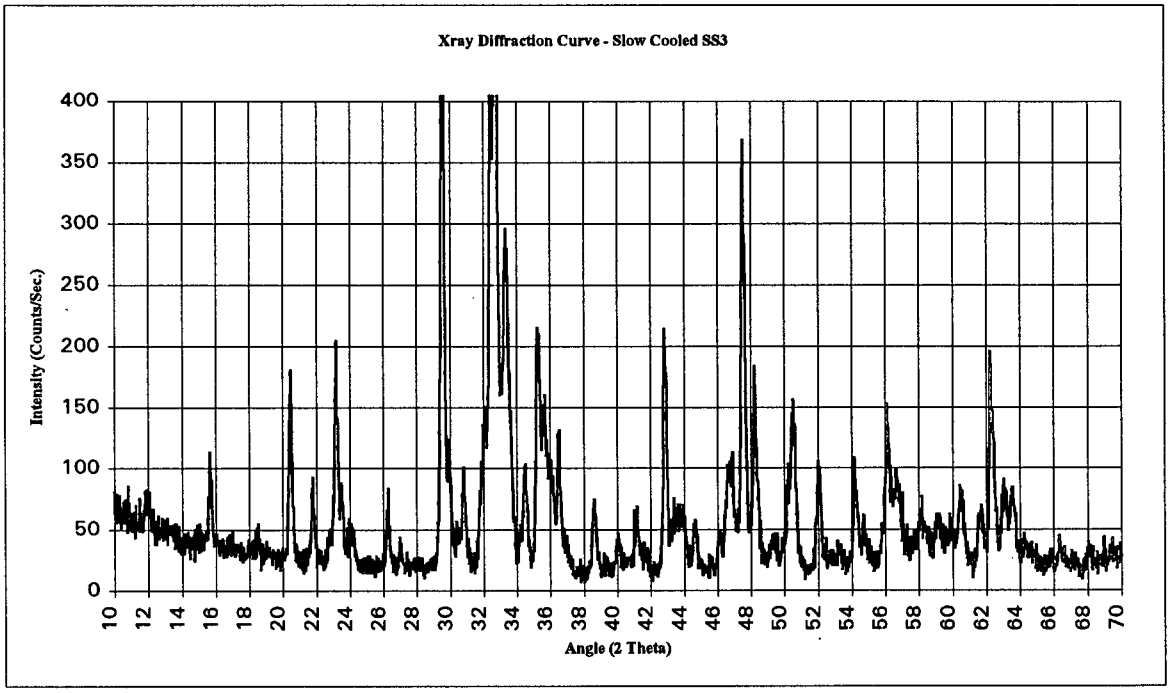

(b)

Figure 17. X-ray diffraction pattern - (a) queched and (b) slow cooled SS3

Figure 18. SEM photograph of quenched SS1

Figure 19. SEM photograph of quenched SS2 (50X)

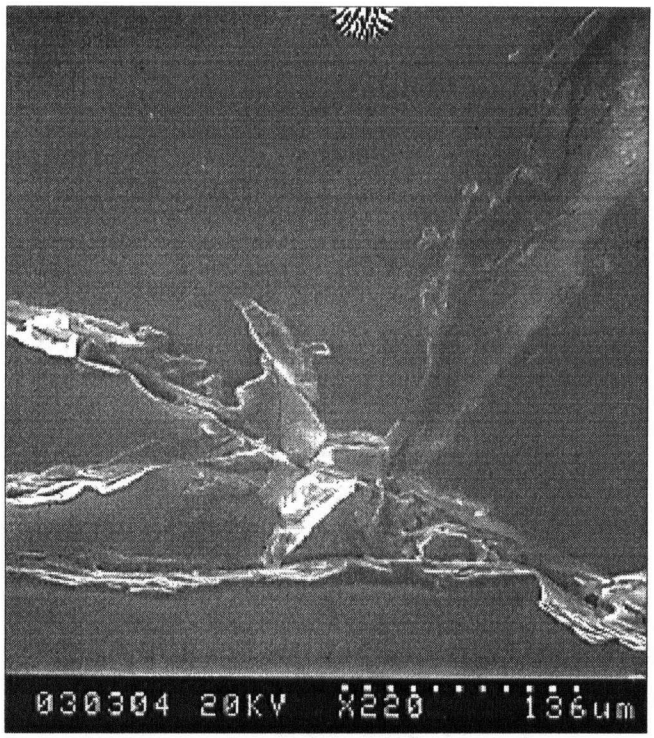

Figure 20. SEM photograph of quenched SS3

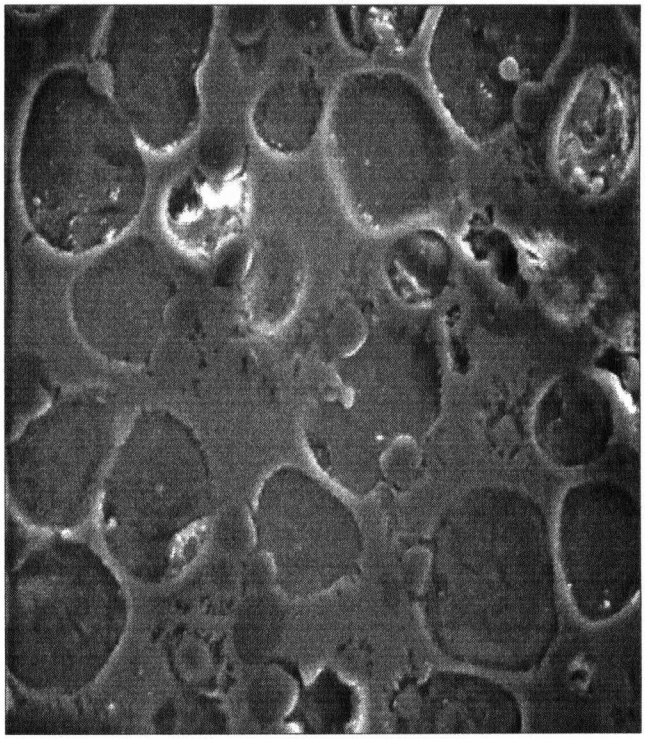

Figure 21. SEM photograph of quenched SS2,
calcium silicates in glassy matrix (1100X)

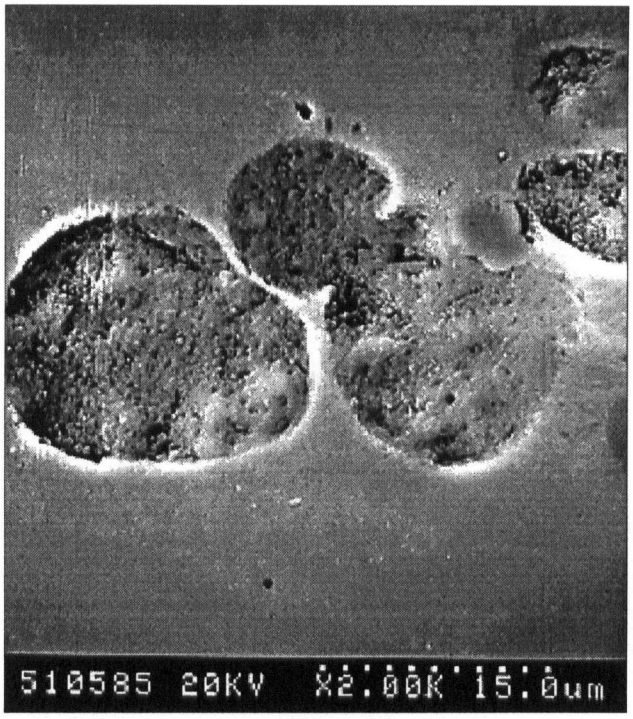

Figure 22. SEM photograph of quenched SS3 calcium silicates in a glassy matrix

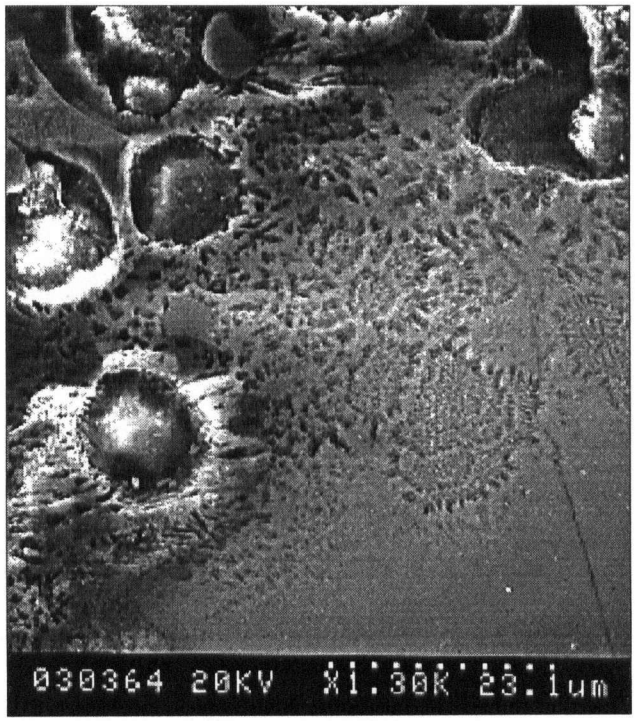

Figure 23. SEM photograph of nucleation and growth of calcium silicates in a glassy matrix

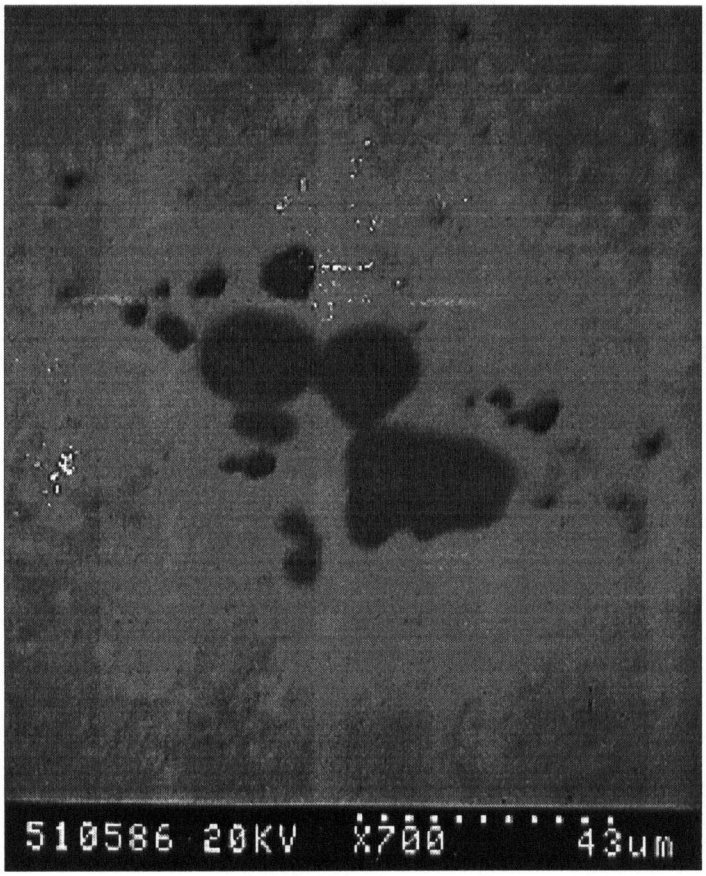

Figure 24. SEM backscattered photograph of periclase in a glassy matrix of quenched synth. slag

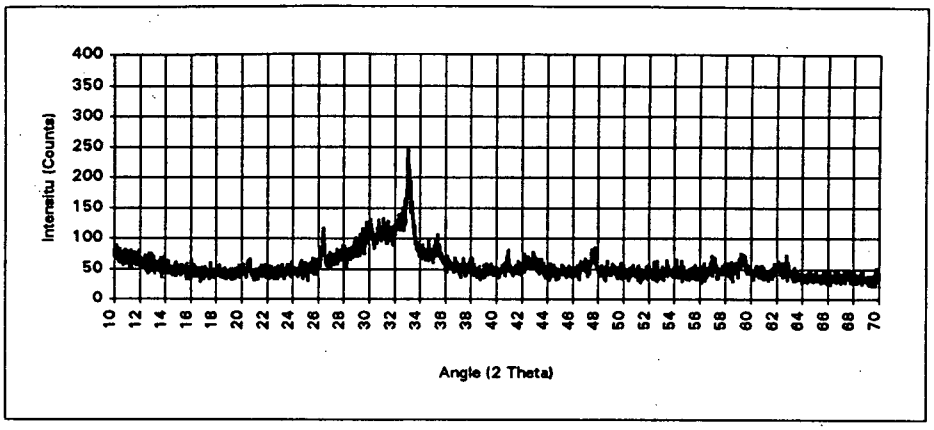

(a)

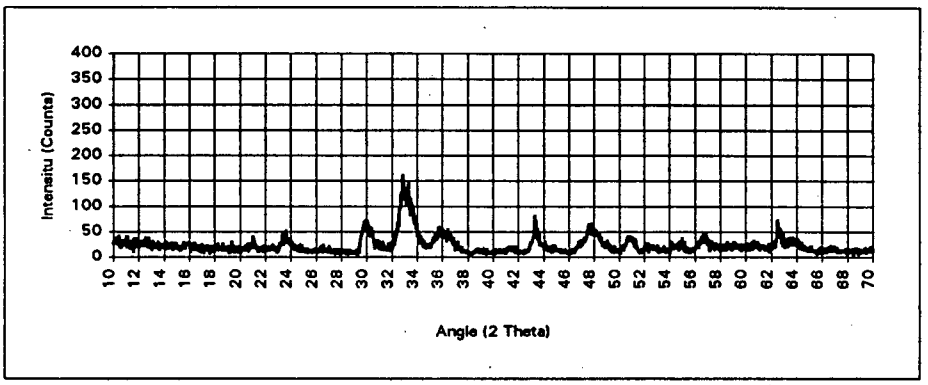

(b)

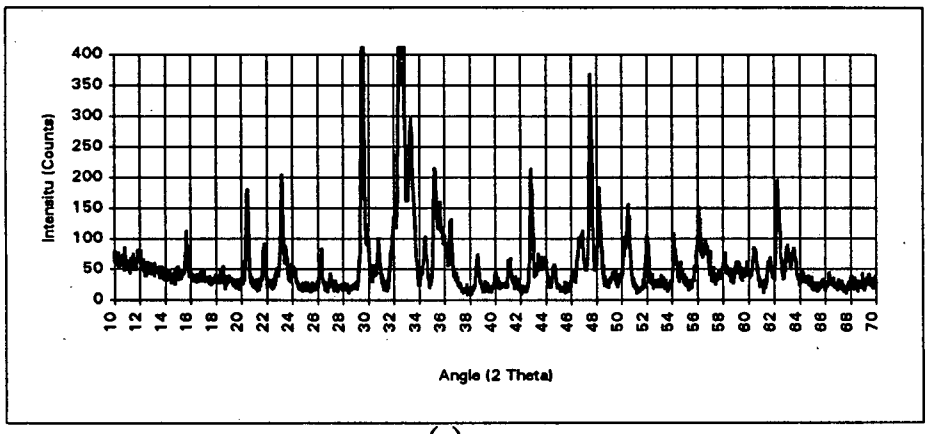

(c)

Figure 25. XRD Pattern for Quenched (a), Rapid Cooled (b), and Slow Cooled mix SS3 (c)

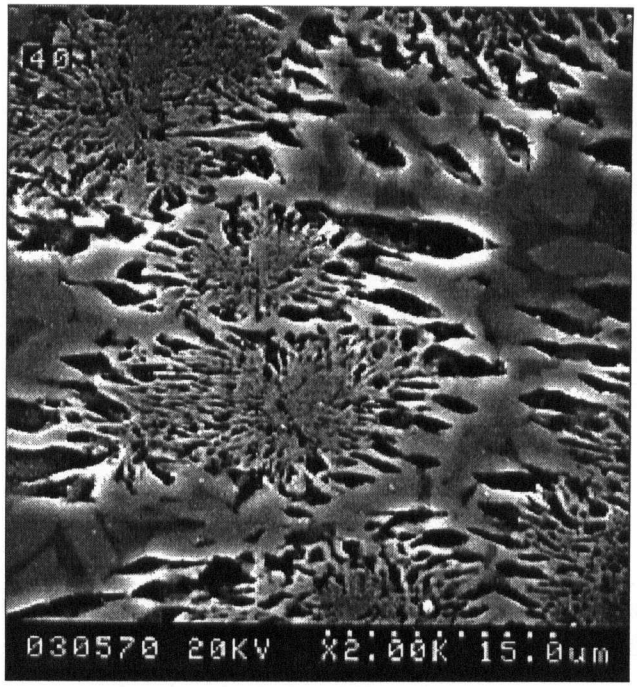

Figure 26. SEM photograph of slow cooled SS1

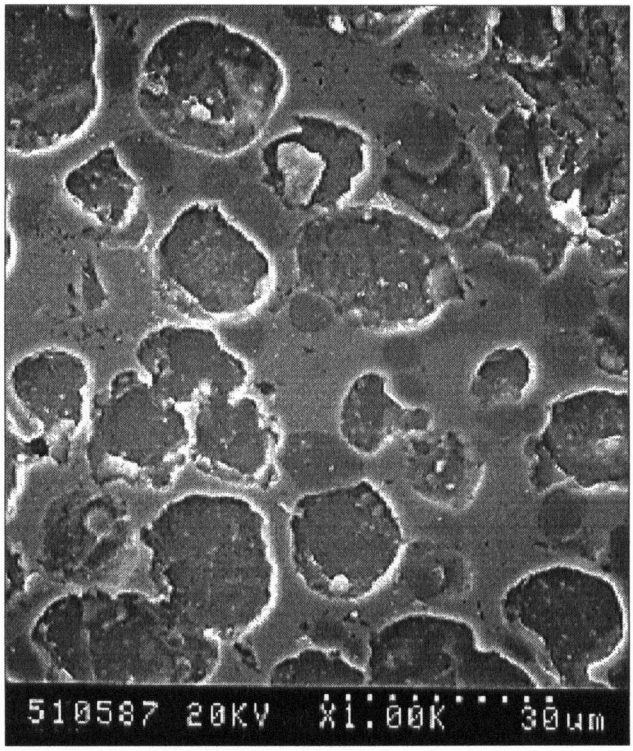

Figure 27. SEM photograph of slow cooled SS2

5.1.2 XRD, EDX, and SEM Analyses of the Stelco Steel Slag

Results from the XRD tests for the Stelco steel slag under varying conditions are illustrated in Figures 28-29. There is a considerable difference in the placement of the peaks in the "as received" slag and the slag that was oxidized at 900°C. The quenched Stelco slag x-ray curve does not possess the characteristic hump found in the synthetic mixes. It may be noted that this granulated material had a glassy appearance compared to the compositionally identical slow cooled material, and broke up easily as did the other quenched synthetic slags.

The XRD of the "as received" (Figure 28(a)) Stelco slag is typical of commercial slags, with characteristic peaks for wustite (magnesio-wustite), calcium ferrite (brownmillerite), and dicalcium silicate. The XRD pattern is similar to the pattern determined by Monaco and Wu [3] for a slow cooled commercial slag. The strong peaks at the 2θ angles 36.5°, 42.5°, and between 60° to 62°, indicate the presence of wustite and magnesio-wustite solid solutions. In the x-ray pattern of the oxidized slag 28(b) (oxidized at 900 °C) the main wustite and magnesio-wustite peaks from 28(a) have disappeared and have been replaced with periclase and magnesio-ferrite peaks, save for the strong peak at 42.5° which is due to the presence of uncombined periclase. The magnesio-ferrite peaks are present at the 2θ angles 30°, 35.5°, 43°, 57°, and 62.5°. Moreover, the calcium alumino-ferrite phase, represented by the peak at 33.5°, is sharper and more intense in the oxidized slag. The calcium silicate peaks remained unchanged after the oxidation of the slag.

The XRD of the oxidized slag in Figure 28(b) clearly indicates that it is possible to alter the wustite solid solutions. Wustite, which is thermodynamically unstable at high temperatures in an oxidizing environment, exists due the equilibrium between Fe, FeO, and Fe_2O_3 during the steel making process. Once the slag is separate from the steel, the FeO becomes unstable and begins to oxidize to a higher valence state, forming Fe_2O_3

The XRD patterns of both oxidized and oxidized and remelted Stelco slag are compared to observe the effect of cooling conditions. The oxidized and remelted Stelco slag

was air cooled and water quenched. The XRD trace of the slow cooled material in Figure 29(b) is very similar to the oxidized Stelco material which had not been remelted. Moreover, the XRD pattern of the oxidized and quenched material, illustrated in Figure 29(a), was comparable to the trace in 29(b). However, the intensity of the peaks is considerably lower, and the width of the peaks has increased, both of which indicate a decrease in crystallinity. The XRD patterns in Figures 28 and 29 represent the case in which the bulk of the FeO in the Stelco slag has been oxidized and formed Fe_2O_3. However, it is not possible to oxidize all the Fe^{2+} to Fe^{3+} in the slag melt. At very high temperature, approximately 1350°C, hematite becomes unstable and begins to dissociate to form magnetite.

The oxidized slow cooled Stelco slag is seen in the micrograph of Figure 30. The dark gray flake-like grains are calcium silicates, surrounded by a calcium ferrite matrix which contains periclase. This slow cooled material differs considerably in appearance from the granulated material in Figure 31(a). Even though these materials differ in appearance, their XRD patterns are similar, which indicates the presence of small cristallites in the quenched Stelco slag. At high magnification, Figure 31(b), it is possible to distinguish the dendritic growth of these crystallites in a glassy matrix.

In general, the slow cooled XRD patterns are consistent with current theory on the formation of certain mineral structures in slags. The formation of C_3S and C_2S occurred as predicted and was indentified in both the slow cooled and quenched specimens. The significant mineralogical difference between commercial slags and the synthetic slags used in this study is the formation of the ferrite phase in the solidified synthetic blends. Wustite solid solutions are predominant in commercial slag systems. However, the wustite solid solutions were eliminated in the remelted Stelco slag due to the oxidation step.

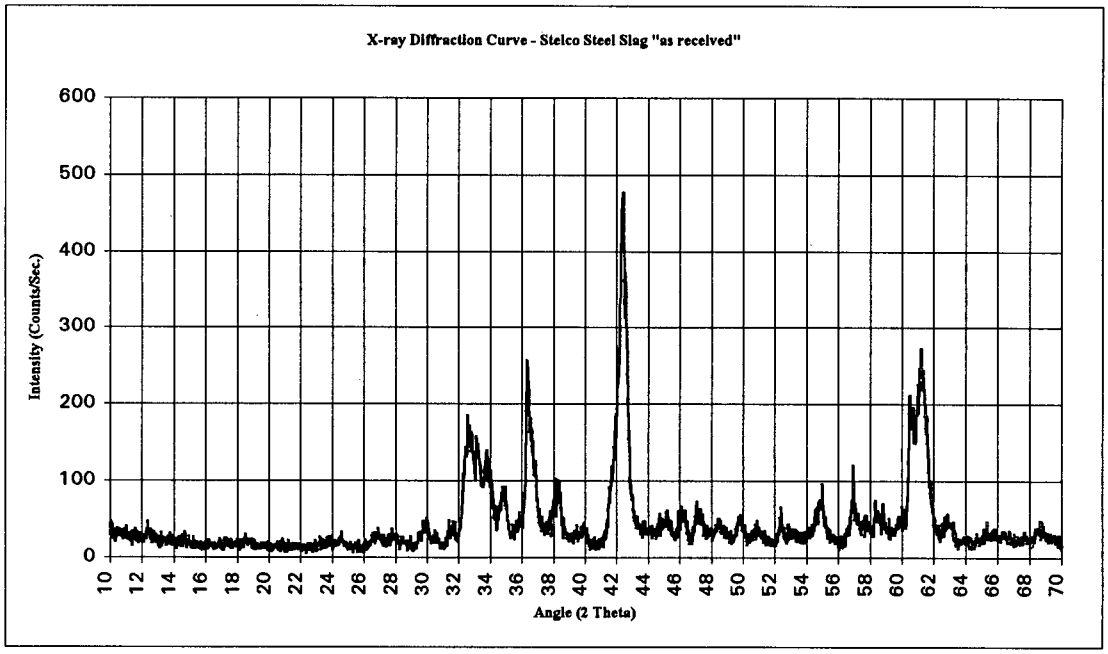

(a)

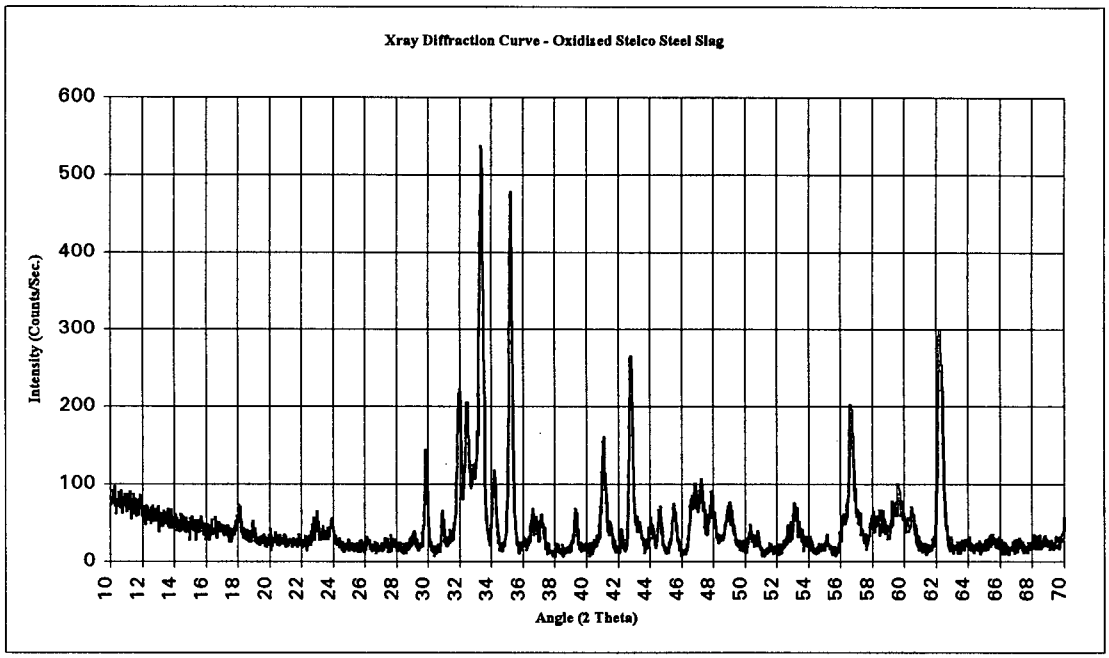

(b)

Figure 28. X-ray diffraction pattern - (a) 'as received' and (b) oxidized Stelco slag

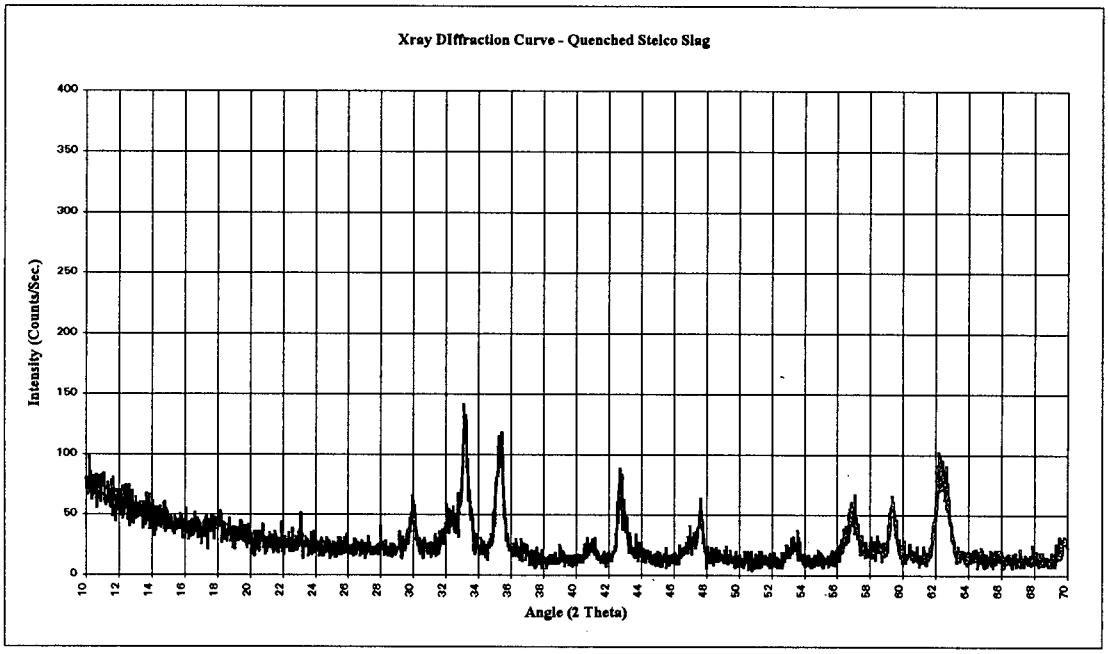

(a)

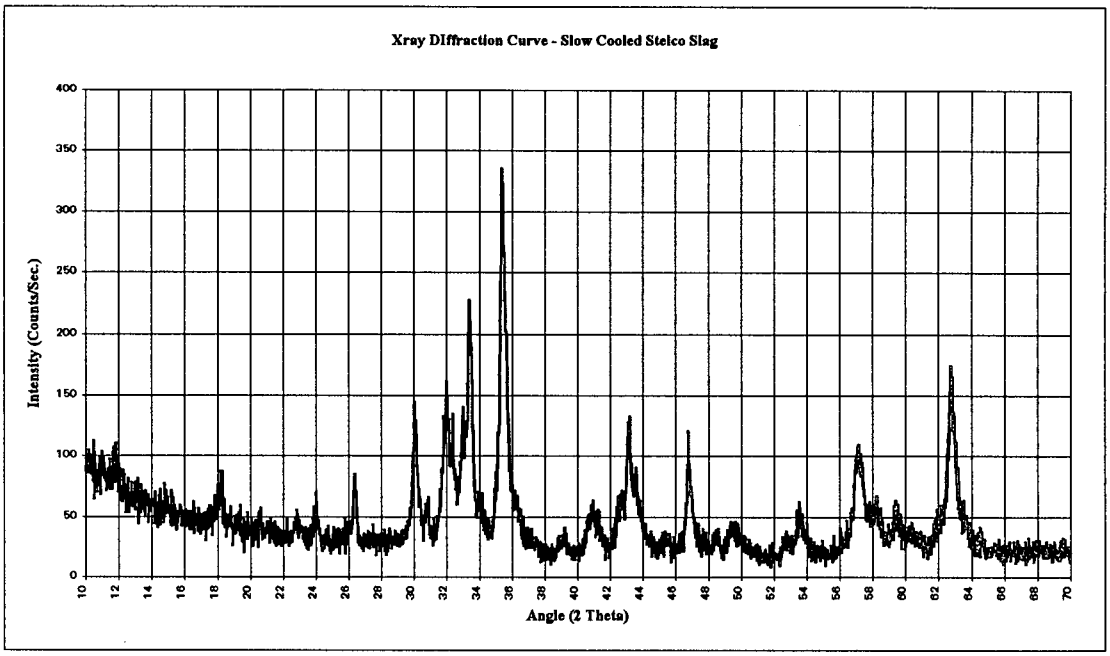

(b)

Figure 29. X-ray diffraction pattern - (a) quenched and (b) slow cooled Stelco slag

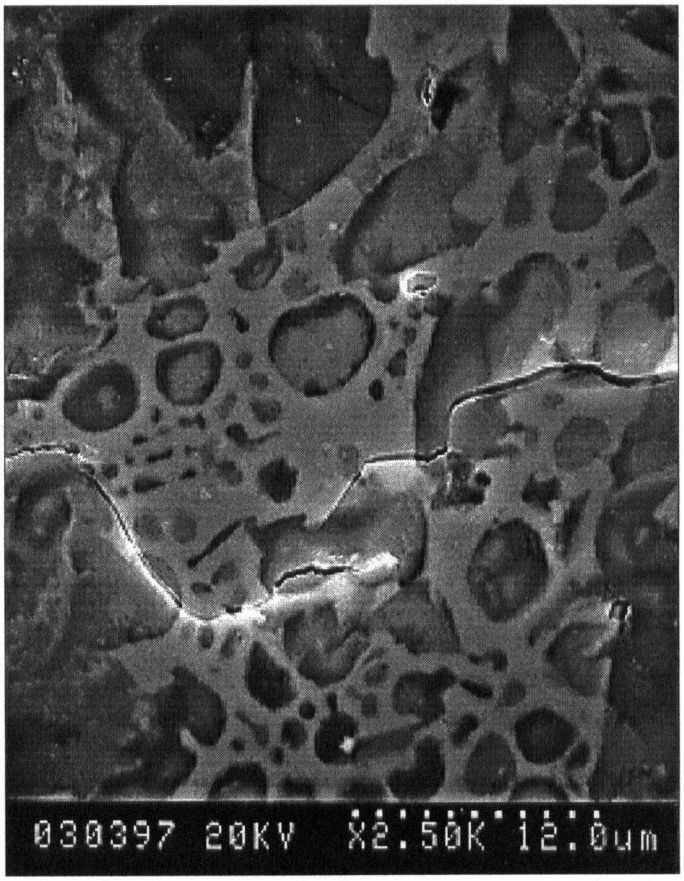

Figure 30. SEM photograph of slow cooled Stelco slag

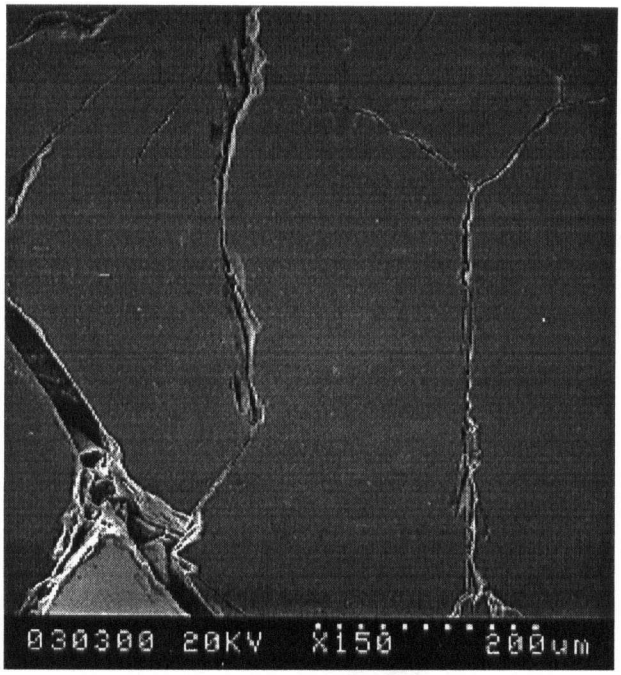

(a)

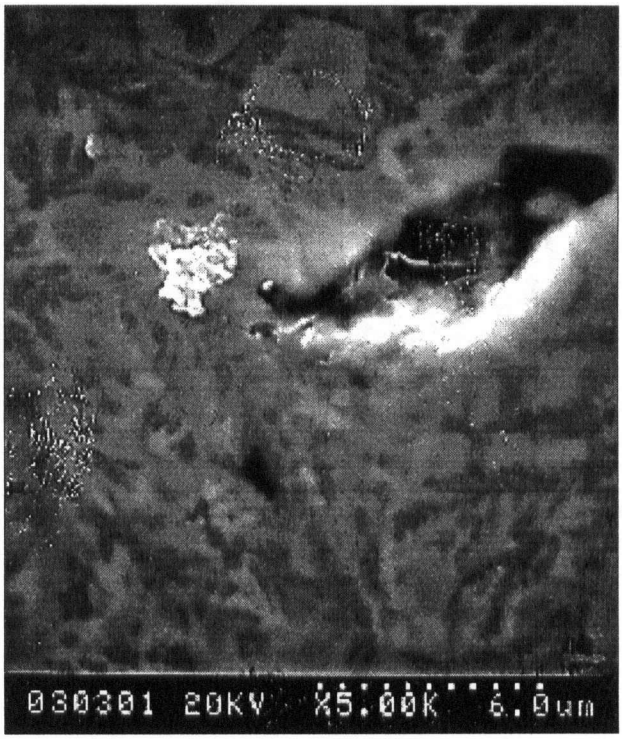

(b)

Figure 31. SEM photograph of quenched (a) amorphous Stelco slag and (b) crystallite growth

5.2 Hydration Study

The purpose of the hydration study was to determine the hydraulic potential of the granulated steel slags. The quenched synthetic mix SS2 and quenched Stelco slags were used for the hydration study. This synthetic mix was chosen because the lime:silica ratio and iron oxide content best represent a commercial steel slag. The slow cooled slags were not used because their extremely high hardness made them too difficult to grind in the ceramic laboratory mill. Furthermore, research [19,20,22,23] indicates that a wide range of glassified slags have been succesfully hydrated to produce cements with excellent long term strength.

Considerable variability was found in the compression test results. This variation may be attributed to a large number of factors during sample preparation. Variables such as the amount of pressure applied to tamp the paste into the mold, the pressure used to remove the cylindrical samples from the mold, laboratory temperature, amount of mold release used in the mold, and general sample quality all had some effect on the final test results. When possible, three samples were tested for each hydration period. In some case the samples did not hold up well and began to crumble around the edges, resulting in lower compression strengths or no result at all. A table illustrating the compression results is given in Appendix I.

5.2.1 Blended Cement Compression Test Results

The compression results of the cements with a 10% steel slag addition appear in Figure 32. The three different A-curves denote the three different steel slags used: A-1 10% Stelco slag melted in a MgO crucible, A-2 10% Stelco slag melted in an Al_2O_3 crucible, A-3 10% synthetic slag (mix SS2) melted in an Al_2O_3 crucible. The graph indicates that the cements with 10% steel slag additions, regardless of which steel slag is used, demonstrate a marked increase in strength for each hydration period. No significant continuous strength

differences or trends in strength may be distinguished between the three different steel slags. The crucial information imparted by this figure is not the actual values of the strength of the blended cements, but rather the general trend of improved strength in the blended cements relative to pure Portland cement.

The compression tests on samples of pure Portland cement and samples with a 10% slag addition were repeated. Compression samples with a 20% steel slag addition using only Stelco slags, were made at this time. This second series of compression tests had higher strengths for both the pure Portland and steel slag addition samples, which reflected some of the variables previously mentioned. However, the same trend in strength persisted in the second series of tests with a 10% slag addition, as seen in Figure 33. The difference in strength between the pure Portland and the slag blended samples was not as pronounced in the second series, but the increase in strength was evident from the first day of hydration through to 35 days. The largest variations in results, relative to the first series of strength test, occurred in the one day tests, which are more sensitive to sample preparation.

Figure 34 presents the strength of blended cements with a 20% slag addition versus the second lot of Portland cement pastes (the second lot of Portland samples were made at the same time as the 20% samples and, therefore, used as the standard). With a 20% slag addition the blended cements maintained, at a minimum, the same strength as the pure Portland samples for each time period. After 14 days of hydration, the steel slag samples began to show a slight increase in strength.

The blended cements with a 45% slag addition demonstrated a significant decrease in strength relative to pure Portland cement, as seen in Figure 35. The significant drop in strength occurs after seven days, with the Portland samples reaching a strength almost double that of the 40% slag samples at this time. However, after the seven day stage the strength of the 40% slag samples began to stabilize relative to that of Portland cement which continues through to 35 day hydration period.

The effect of slag addition on the strength of Portland cement for a series of hydration times is portrayed in Figure 36. The values of strength were averaged and normalized versus pure Portland cement to produce this graph. A significant trend denotes a maximum increase in strength with 10% slag addition. This increase suggests a synergystic effect on compression strength at this ratio of cement to steel slag. The strength falls to no less than 100% of the strength of Portland with a 20% slag addition. Finally, at 40% slag the strength of the blended cement drops significantly relative to that of Portland cement for the hydration periods tested.

The compression samples with a 1:1 ratio of blast furnace slag to steel slag had relatively weak strength relative to Portland cement. Figure 37 depicts the results for the case of a blended cement with a combined slag content of 50% activated with 10% gypsum. Even though the strengths are not comparable to those of Portland cement they do rival those of the samples with 40% steel slag addition shown in Figure 35. It is not clear from these results what effect the slags had on each other's strength performance in the blended cement. There is no evident symbiotic effect between the two slags as was theorized by Montgomery and Wang [15]. However, this symbiosis had been presumed for a blend of granulated blast furnace slag and for slow cooled "weathered" steel slags, not for granulated steel slag.

Theory suggests that predominantly glassy blast furnace and steel slags would have better long term strength, eventually reaching that of Portland cement after several months. The only sample to approach such a trend is D-3 in Figure 37, which has a greater increase in strength at 35 days than the samples D-1 and D-2. This increase is attributable to the higher glass content of the quenched synthetic steel slag SS2.

At higher combined slag contents, 80% blast furnace and steel slag, the samples made with synthetic slag S.S.5 had improved strength at each hydration stage relative to the samples made with the commercial Stelco slag, Figure 38. The strength results in Figure 38 suggest that at each time stage the samples E-3, made with the more glassy SS2 slag, have improved strength compared to the sampes E-1 and E-2, made with less amorphous quenched

Stelco slags. This indicates that at extremely high slag contents, the amount of glassy material directly affects the strength properties of the cement. This has been shown to be the case in ground granulated blast furnace slag cements [22].

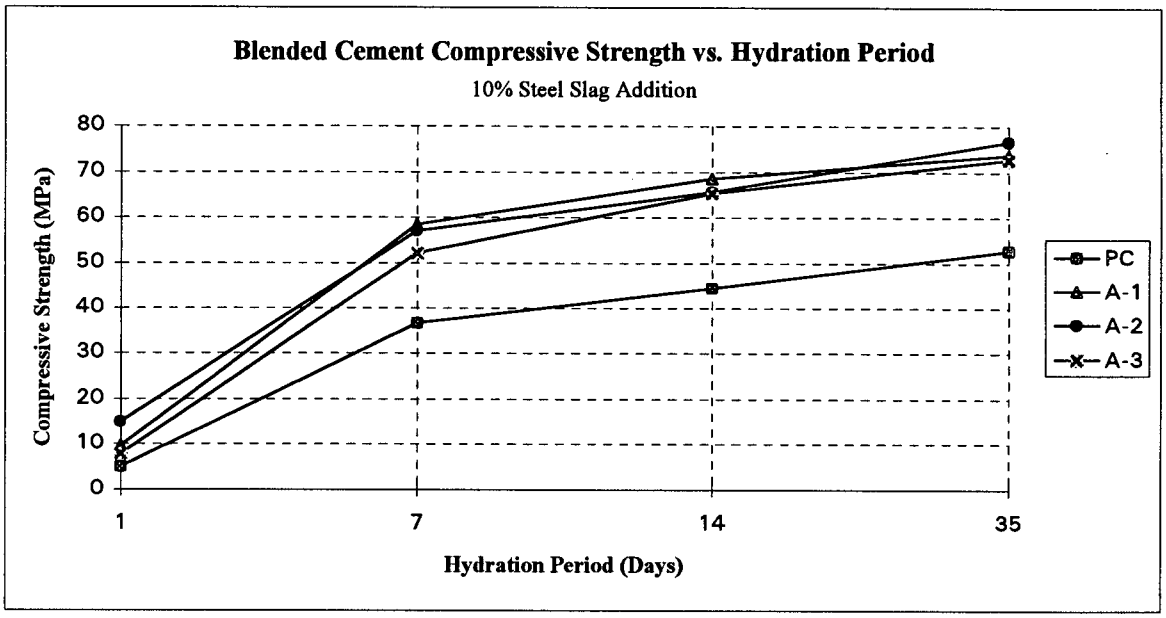

Figure 32. Compressive Strength of 10% Steel Slag Blended Cements

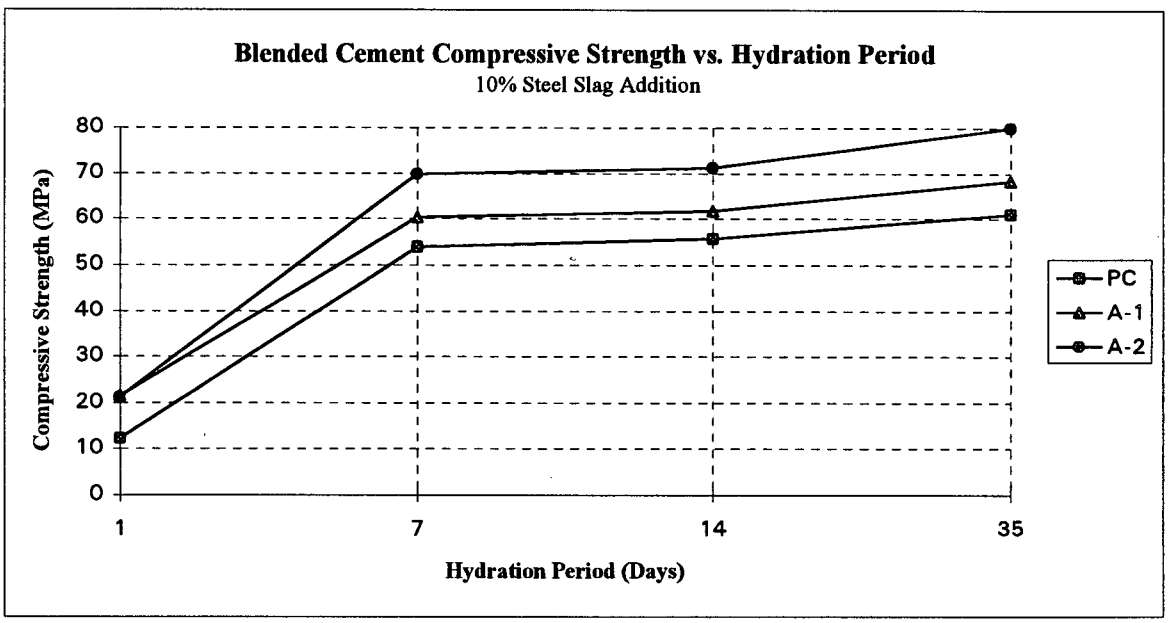

Figure 33. Compressive Strengths of 10% Steel Slag Bleneded Cements
Second Series of Test Samples

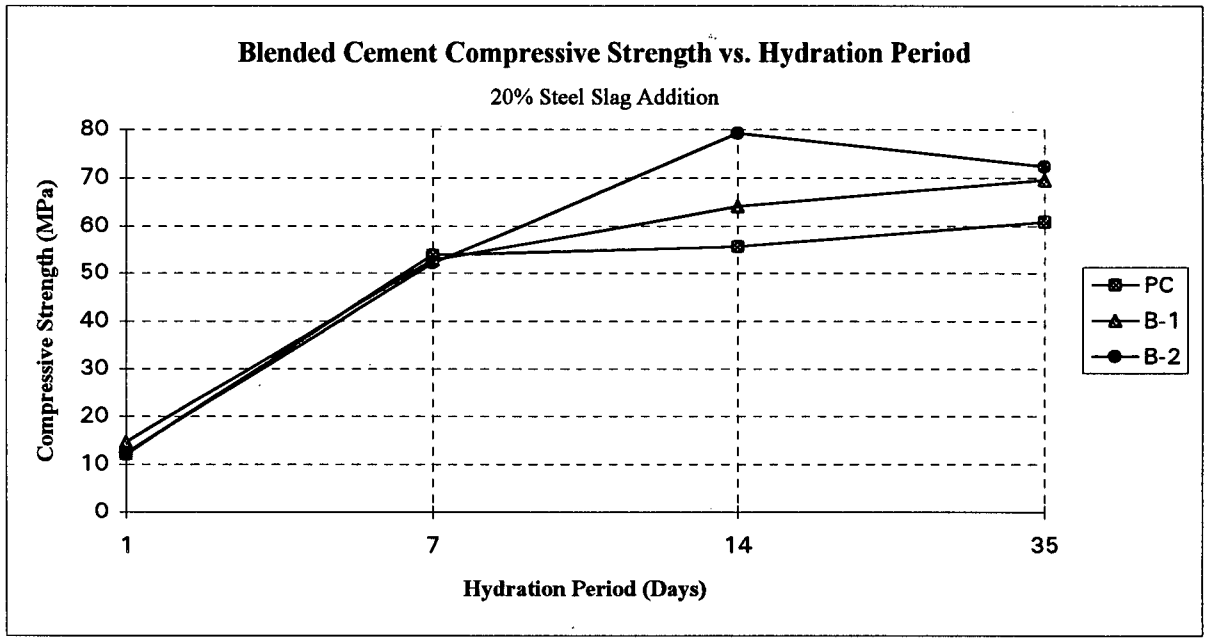

Figure 34. Compressive Strengths of 20% Steel Slag Blended Cements

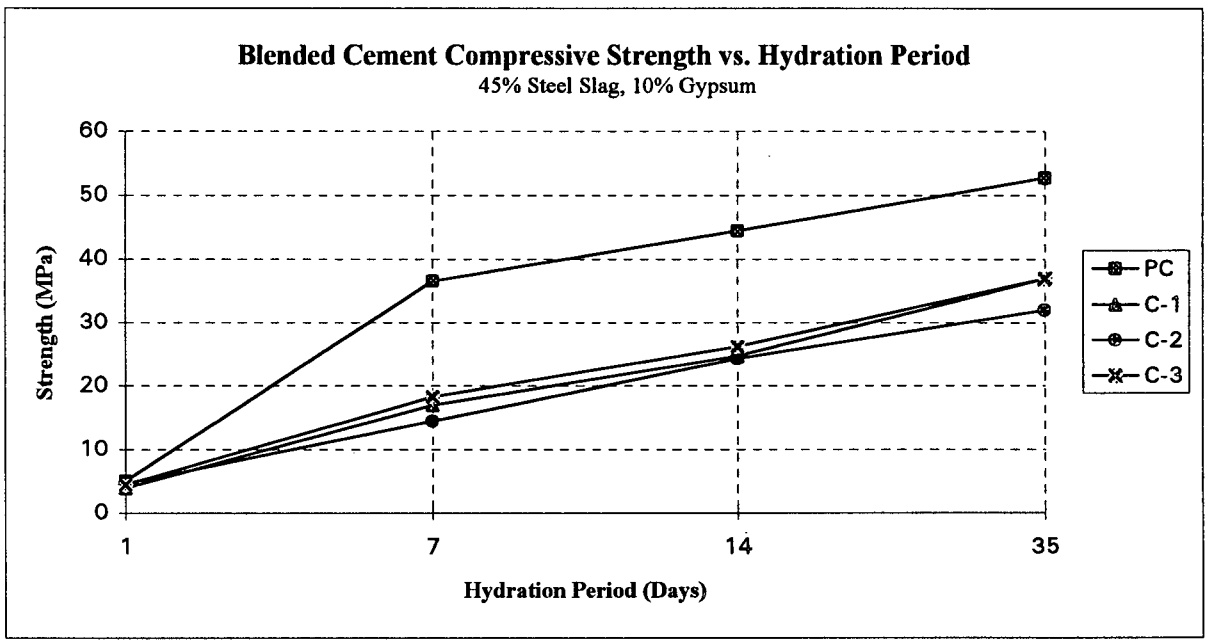

Figure 35. Compressive Strengths of 45% Steel Slag, 10% Gypsum Blended Cements

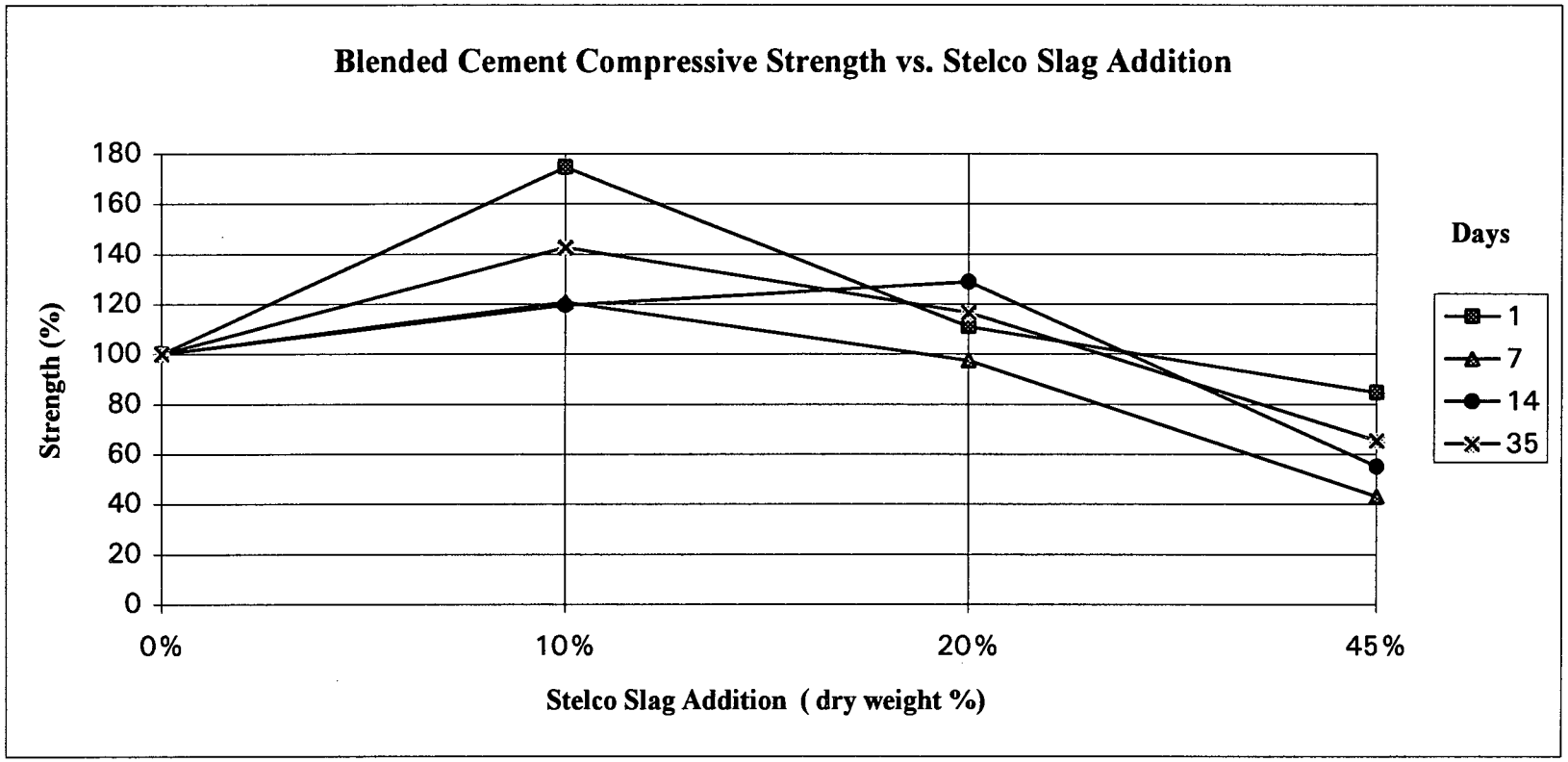

Figure 36. Compressive Strengths versus Steel Slag Addition

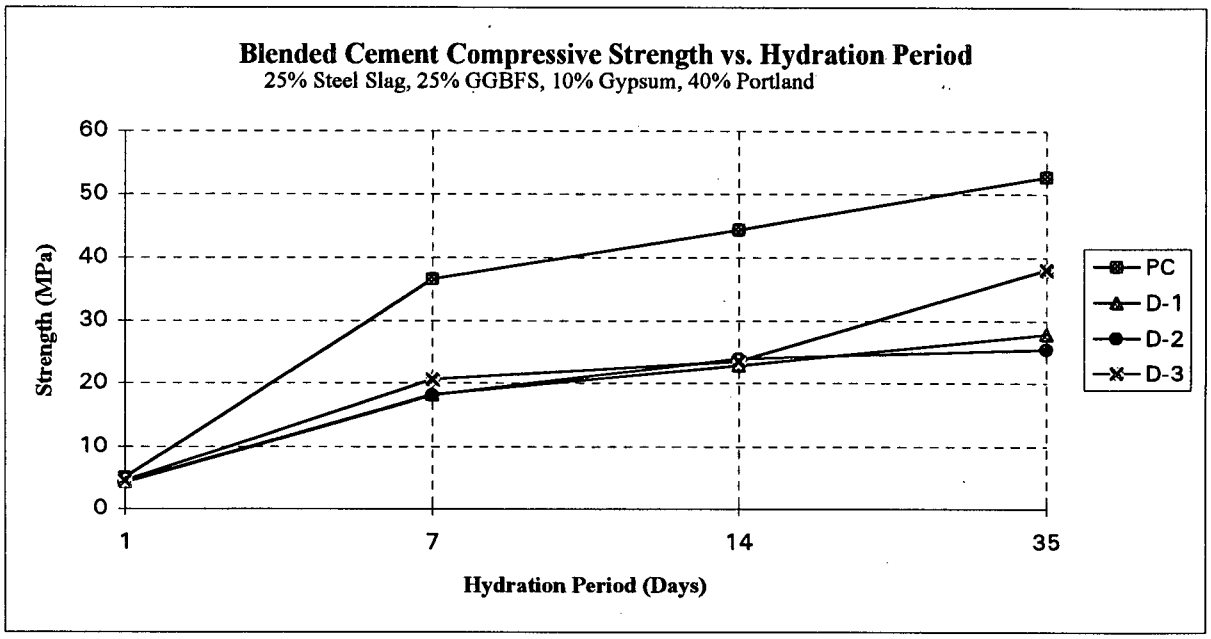

Figure 37. Compressive Strengths of 25% Steel Slag, 25% GGBFS, 10% Gypsum, 40% Portland Blended Cements

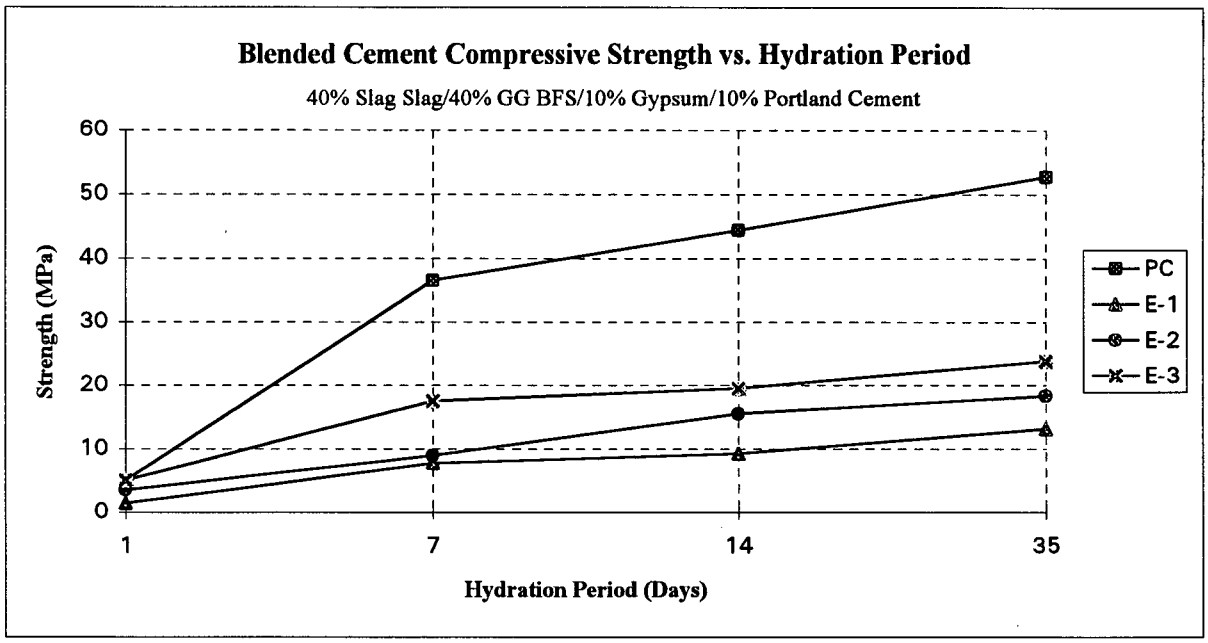

Figure 38. Compressive Strengths of 45% Steel Slag, 45% GGBFS, 10% Gypsum, 10% Portland Blended Cements

5.2.2 X-ray Diffraction Analyses of Hydrated Portland and Blended Cements

XRD analyses were performed on the hydrated Portland and blended cements for hydration periods of 1, 7, and 14 days. The XRD traces were carried out in an effort to determine the effect of 10% and 20% Stelco steel slag addition on the hydration and subsequent cementitious properties of Portland cement. The analysis of the differing diffraction patterns allowed for the comparison of the crystalline peaks, depending on slag addition, and the change in these peaks due to the length of the hydration period.

The primary hydration products produced during the hydrolysis of the calcium silicates in a Portland cement are a C-S-H rigid gel and calcium hydroxide (CH). The C-S-H gel is primarily amorphous or poorly crystalline, making it difficult to detect using XRD techniques [28]. It is possible to ascertain the amount of C-S-H gel produced during the hydration of pure tricalcium silicate by using QXRDA to determine the amount of crystalline tricalcium silicate that has reacted in the paste. However, this technique becomes much more difficult during the hydration of Portland cement due to the interaction of the numerous hydration products present in the paste. The other hydration product CH forms a crystalline layer structure, similar to that of Portlandite, and dissolves in water at room temperature [28].

The diffraction pattern of a 23 year old belite paste is shown in Figure 39. This diffraction trace is very similar to that of a fully hydrated alite paste. The only sharp crystalline peaks are attributable to CH, while the diffuse peaks are the result of the C-S-H gel [28]. The sharp peaks of the calcium silicates that are present in the cement clinker (Figure 12), between the 2θ angles 29° and 35° have been replaced by the diffuse C-S-H hump in Figure 39. As the calcium silicates continue to hydrate during the long term performance stages of the cement, the crystalline material is continuously replaced by the amorphous C-S-H rigid gel.

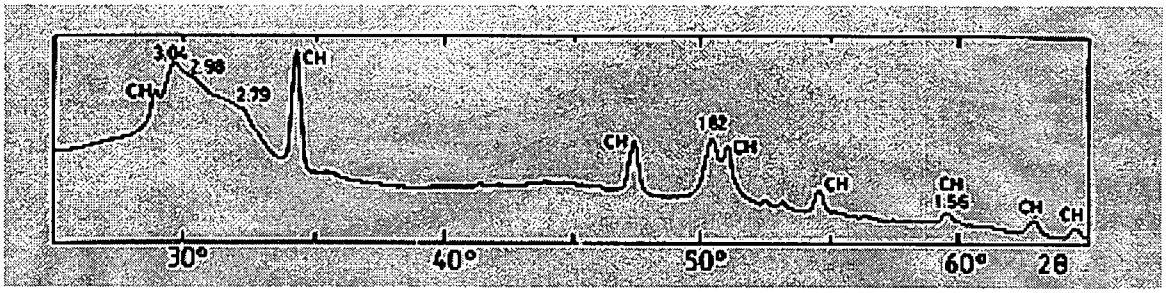

Figure 39. XRD Pattern of a Fully Reacted Belite Paste [28]

The XRD traces of a hydrated Portland cement paste over the period of 14 days are shown in Figure 40. The XRD pattern for the 1 day hydration period has changed very little compared to the anhydrous cement in Figure 12. The most important change to note is the decrease in intensity of the calcium silicate, calcium aluminate, and calcium alumino-ferrite peaks in the hydrated paste. These peaks continue to decrease in intensity as their associated crystalline phases continue to hydrate over time. The calcium aluminate and calcium alumino-ferrite peaks at 33° and 33.9° 2θ respectively, have all but disappeared after one day of hydration. This is to be expected as these compounds hydrate rapidly relative to the calcium silicates [1].

The amorphous hump present between the 2θ angles of 16° and 28° in the cement clinker XRD pattern of Figure 12 has disappeared. However, a new peak has formed in the hydrated paste at 18.5° 2θ, which has increased in intensity by 7 days and remains constant up to 35 days of hydration. This peak is attributable to the formation of calcium carbonate which is known as Portlandite and is a by-product of the hydration process. In general, all the peaks in the hydrated paste have dropped in intensity and have become more diffuse after 1 day of hydration. This trend will continue over time until all the compounds have fully hydrated, eventually yielding an XRD trace similar to that in Figure 39.

Figure 41 shows the XRD traces of a 10% Stelco steel slag blended cement hydrated over a period of 14 days. The important trend to note is the reduction in peak intensity and

the growth of an amorphous hump between the 2θ angles of 28° and 36° as the hydration period lengthens. The increase in intensity of the Portlandite peak at 18.5° 2θ over time is the only other significant change in the XRD traces in Figure 41. The XRD traces of a 20% Stelco slag blended cement for a hydration period of 14 days are shown Figure 42. The intensity of the peaks in this figure is similar to those of the pure Portland cement paste in Figure 40. The only apparent difference is the appearance of the Portlandite peak after 1 day which did not occur in either the Portland cement or 10% blended cement.

The effect of slag addition on the XRD pattern after 1 day of hydration is shown in Figure 43. The significant difference in the XRD patterns after 1 day of hydration is the relative intensity of the peaks. The blended cement with 10% slag addition has the highest intensity of the calcium silicate peaks. The intensity of the Portlandite peak is the greatest in the 20% steel slag blended cement and does not appear in the other cements until later hydration times. The presence of a peak 35.9° 2θ may also be detected in the 20% slag sample and is not present in the other traces of Figure 43. However, this peak was detected at later hydration times in both Portland cement and the 10% slag blended cement, as seen in Figures 40 and 41.

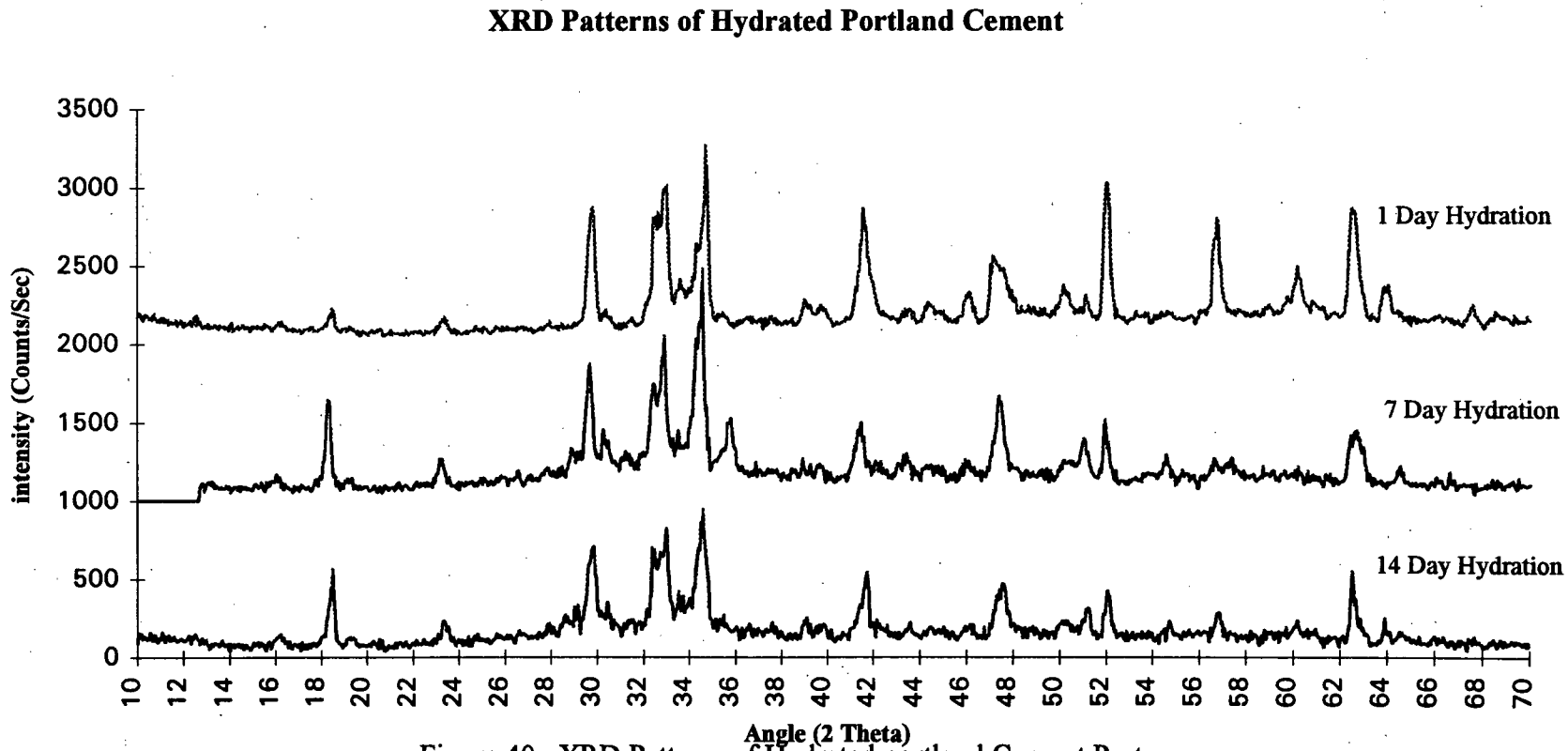

Figure 40. XRD Patterns of Hydrated portland Cement Paste

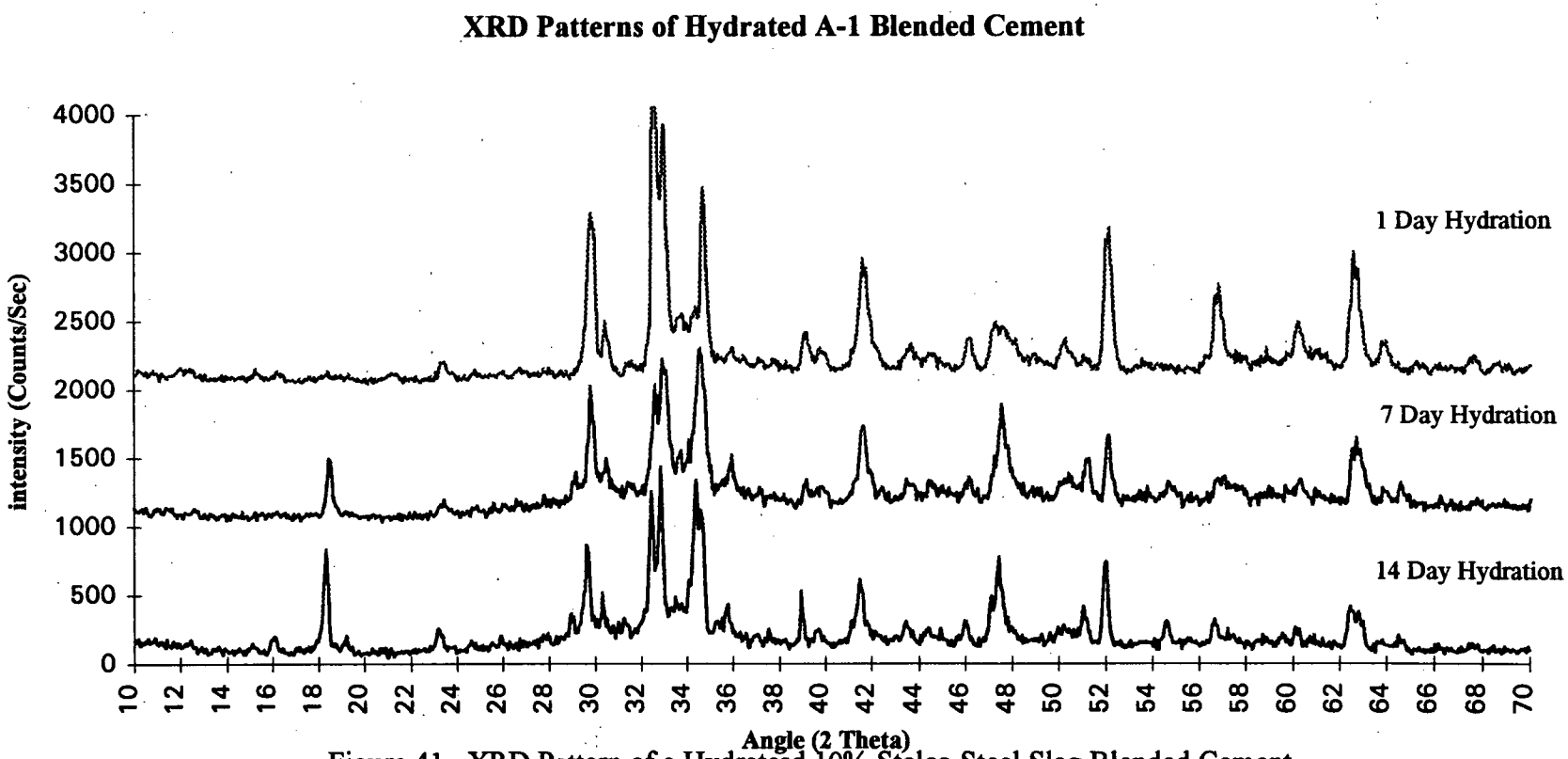

Figure 41. XRD Pattern of a Hydratesd 10% Stelco Steel Slag Blended Cement

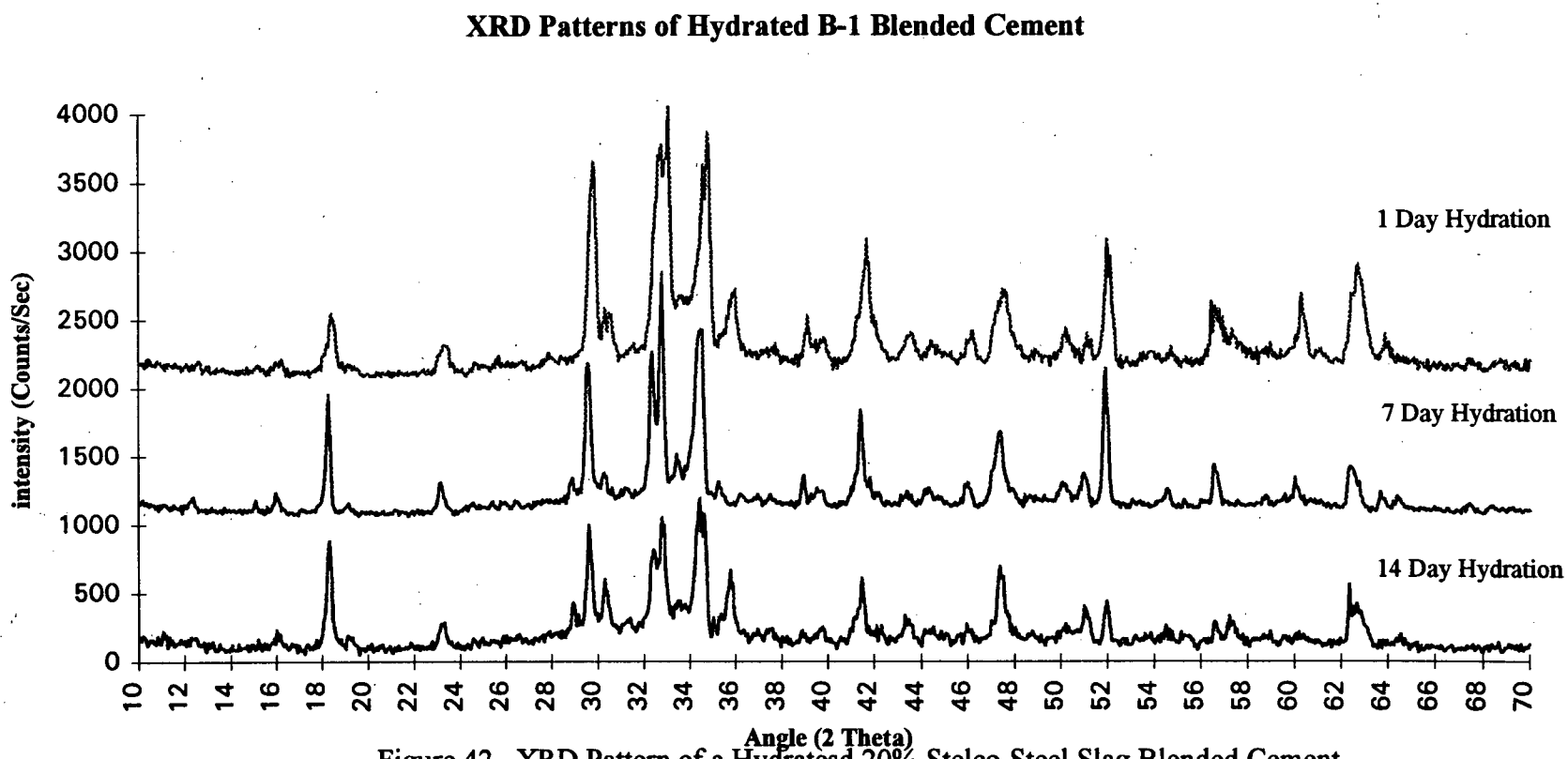

Figure 42. XRD Pattern of a Hydratesd 20% Stelco Steel Slag Blended Cement

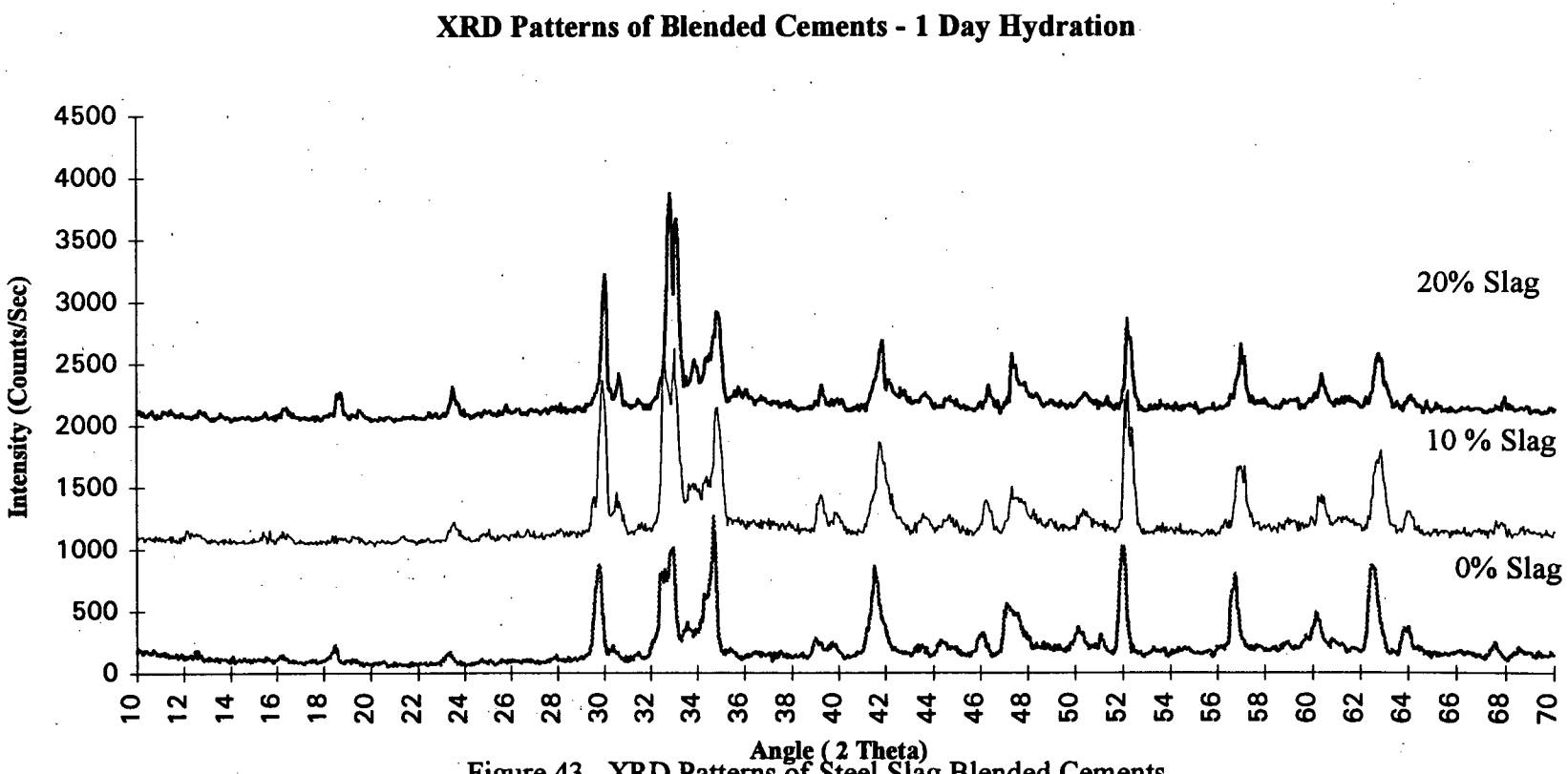

Figure 43. XRD Patterns of Steel Slag Blended Cements

6.0 CONCLUSIONS

The processing conditions of steelmaking slag were optimized to improve the hydraulic nature of the material to a level which allowed for its blending with conventional Portland cement clinker. The desired results were achieved through minor adjustments in liquid slag chemistry, the principle adjustment being the oxidation of FeO to Fe_2O_3. Furthermore, the slag was rapidly quenched obtaining a predominantly amorphous material containing the principle phases of Portland cement. Despite the high lime to silica ratio of the slags, which is not conducive to glass formation, by rapidly quenching the molten slag it was possible to freeze its liquid structure, thereby inhibiting nucleation and crystal growth.

The oxidation of the bulk of the bivalent iron to trivalent iron in the molten slag proved to be an integral processing step in enhancing a slag's cementitious properties. The oxidation step was primarily aimed at reducing the amount of wustite, and its solid solutions, which are the main composition variable in the slag, and behave as diluants in blended cements. By raising the oxidation state of the bivalent iron to the trivalent form, it was possible to obtain cementitious minerals in the slow cooled slags. According to the CaO-Al_2O_3-Fe_2O_3 ternary phase diagram, the trivalent iron was able to combine with calcium and alumina to produce a ferrite phase upon cooling from the melt. The ferrite phase, having a median composition of brownmillerite C_4AF, is one of the major mineral phases found in Portland cement and hydrates readily when mixed with water. Therefore, by oxidizing the slag it was possible to convert a harmful mineral phase into a strength contributing compound in the slow cooled slags.

In the case of the granulated slags the trivalent iron did not have time to precipitate out of the melt to form ferrite minerals, and was subsequently frozen into an amorphous solid. The increase in trivalent iron present in the slag melt, due to oxidation, improved the glass forming potential by effectively reducing the basicity of the liquid slag. In the molten

slag, a shift in ionic structure from the orthosilicate composition towards larger more complex ionic rings is attributable to the increase in trivalent iron. Some of the trivalent iron acts as a network former, thereby decreasing the O:Si (basicity) ratio of the complex ions in the melt. The bivalent iron, however, behaves only as a network modifier and promotes the formation of small orthosilicate ions which are more apt to crystallize upon cooling . Therefore, by dramatically shifting the ratio of Fe^{2+}/Fe^{3+} ions in the melt, the effective basicity has been reduced, promoting the glass forming potential of the molten slag.

The cooling rate had a significant effect on the final structure of the solidified slag. The XRD analysis indicated that controlled cooling of the liquid slag promoted the formation of the main cementitious minerals: alite, belite, calcium aluminate, and calcium alumino-ferrite. However, by rapidly quenching the liquid slag it was possible to produce a predominantly glassy material that possessed inherent cementitious potential. The processing combination of oxidation and granulation successfully produced an easily ground amorphous solid with suitable hydraulic properties.

The blending of slag with Portland cement had a notable impact on compressive strength (over a 35 day hydration period) depending upon the amount of slag added. At a low steel slag addition of 10%, a marked increase in strength was observed over that of pure Portland cement for each hydration period. With a 20% steel slag addition, the strength of the blended cement rivaled that of pure Portland cement for the hydration periods tested. However, at high slag additions of 40% the strength of the blended cement demonstrated a significant reduction in strength. The 10% steel slag blended cement produced the maximum increase in strength. This increase is due to a synergistic effect between the hydrated slag and Portland cement.

The high iron oxide content of the slag addition resulted in an increase in the amount of ferrite phase in the blended cement. This ferrite phase, which hydrates rapidly and to completion over a short period of time, could have ensured an increase in short term strength in the hydrated pastes. Futhermore, the presence of crystallites of alite and belite in the

amorphous granulated slag would have the ability to hydrate readily due to their large surface area, thereby contributing to the long term strength of the blended pastes.

This research indicates that properly processed steel slag may be blended with cement clinker in a 1:10 ratio and effect an increase in the strength of Portland cement. At slag additions as high as 20% the strength of blended cement paste is comparable to that of pure Portland cement over a 35 day hydration period. These results are encouraging and suggest that, by relatively minor processing of steel slag in the liquid state, a useful, value-added product can be obtained from what at present is a waste product.

7.0 FUTURE WORK

There is much fundamental research which needs to be conducted before the commercial production of steel slag blended cements becomes a viable process. Several key theoretical and practical issues will have to be investigated and resolved to ensure that the large scale recycling of steel slag becomes a reality.

I) The limited number of synthetic slags used in the present work had iron oxide contents ranging from approximately 22% to 29 % by weight. Since steel slags can very widely in iron content, it would be of interest to perform a series of melts using synthetic slags with a wide range of iron oxide content. Such a sample range would allow for the assessment of varying iron oxide contents on glass formation and the subsequent effect on the cementitious properties of a blended cement. Furthermore, the determination of a maximum and minimum iron oxide content, would establish compositional limits for slags which could be successfully be processed for use as a cement additive.

II) The variability in the data from the compression study made it difficult to state conclusively, with statistical accuracy, any actual values of strength of the blended cements. By expanding the sample size and repeating several tests at various times it would be possible to quote statistically valid strength values for the blended cement pastes. Since only one commercial slag was used through out this study it would be of interest to expand the sample group to include other steelmaking slags. Moreover, strength tests over longer hydration periods are necessary to ensure that blended cements possess good long term strength.

III) All the compression tests in this study were performed on cement pastes. Therefore, the next step in developing a saleable product dictates that tests on concrete be

performed, as concrete, and not cement paste, is the construction material used commercially. This type of investigation would explore the slag-aggregate interaction in the blended material, which is critical in alkali environments such as salt water applications.

IV) Investigating the viability of processing electric arc furnace slag in the same manner is of interest, since mini mills, which use EAFs, produce a considerable amount of waste product from their steelmaking operations. The EAF slag is similar in composition to that produced by the BOF process. However, it has a higher lime content which may inhibit glass formation.

REFERENCES

1. F. M. Lea, The Chemistry of Cement 3rd edition, Edward Anarnold Publishers Ltd, Glasgow, Great Britain 1970.

2. J. Geisler, "Steel Slag- "Generation, processing and utilization"", Proceedings of the International Symposium on Resource Conservation and Environmental Technologies, pp. 87-94, Aug., 1994.

3. A. Monaco and W-K. Wu, "The Effect of Cooling on the Mineralogical Characterization of Steel Slag", Proceedings of the International Symposium on Resource Conservation and Environmental Technologies, pp. 107-116, Aug., 1994.

4. J.J. Emery and B. L. Ferrand, "Recent Improvements in the Quality of Steel Slag Aggregate", Proceedings of the International Symposium on Resource Conservation and Environmental Technologies, pp. 99-106, Aug., 1994.

5. P. Barnes, Structure and Performance of Cements, Applies Science Publishers, 1983.

6. G. C. Bye, Portland Cement: composition, production, and properties 1st edition, Institute of Ceramics Pergamon Press, Oxford, Great Britain 1983.

7. R. W. Nurse, "Phase Equilibria and Constitution of Protland Cement Clinker", 4th International Symposium on the Chemistry of Cement, Washington D.C., Paper II-1, 1960, pp. 9-33.

8. H. G. Midgley, D. Rosaman, and K. E. Fletcher, "X-ray diffraction Examination of Portland Cement Clinker", 4th International Symposium on the Chemistry of Cement, Washington D.C., Paper II-S2, 1960, pp. 69-81.

9. L. R. Nelson, "Determination of the Possible Causes of a Foaming Slag by its Mineralogical and Textural Characterization", Extraction and Processing for the Treatment and Minimization of wastes, 1993, pp. 1041-1062.

10. F. Wachsmuth, J. Geisler, W. Fix, K. Koch, and K. Schwerdtfeger, "Contribution to the Structure of BOF-Slags and it's Influence on their Volume Stability", Canadian Metallurgical Quarterly, Vol. 20, No 3, 1981, pp. 279-284.

11. G. H. Thomas and I.M. Stephenson, " The Beta to Gamma Dicalcium Silicate Phase transformation and its significance on air-cooled slag stability", Silicates Industrielles, 1978-9, pp. 195-200.

12. S. S. Shan and Y. Yushu, "Study of Steel Slag Cement", Silicates Industrielles, 1983-2, pp. 31-34.

13. N. A. Toropov, "Solid Solutions on the Minerals of Portland Cement Clinkers", 4th International Symposium on the Chemistry of Cement, Washington D.C., Paper II-S7, 1960, pp. 113-118.

14. F. W. Locher, "Solid Solution of Alumina and Magnesia in Tricalcium Silicate", 4th International Symposium on the Chemistry of Cement, Washington D.C., Paper II-S5, 1960, pp. 99-103.

15. D. G. Montgomery and G. Wang, "Preliminary Study of Steel Slag for Blended Cement Manufacture", Materials Forum , Vol.15, 1991, pp. 374-382.

16. Y. Wang and D. Lin, "The Steel Slag Blended Cement", Silicates Industrielles, Vol. 6,1983, pp. 121-126.

17. S. S. Sun and Y. Yuan, " Study of Steel Slag Cement", Silicates Industrielles, Vol. 2, 1983, pp. 31-34.

18. T. Idemetsu, S. Takayama, and A. Watanabe, " Utilization of Converter Slag as a Constituent of Slag Cement", Trans. Japan Concr. Inst., Vol. 3, 1981, pp. 33-38.

19. D. M. Roy and G. M. Idorn, "Hydration, Structure, and Properties of Blast Furnace Slag Cements, Mortars and Concrete", ACI Journal, Vol. 79-43, 1982, pp. 444-457.

20. R. Coale, C. W. Wolhuter, P.R. Jochens, and D.D. Howat, "Cementitious properties of Metallurgical Slags", Cement and Concrete research, Vol. 3, 1973, pp. 81-92.

21. J. Zarzycki, Glass and the Vitreous State, Cambridge University Press, Cambridge, Great Britain 1991.

22. F. Schroder, "Blast Furnace Slags and Slag Cements", Session IV-3 Slags and Slag Cements, SESSION IV-3, 1960, pp. 149-195.

23. D. Roy, Hydration, "Microstructure, and Chloride Diffusion of Slag Cement Pastes and Mortars", Trodheim Conference, Norway, 1989, pp. 1265-1280.

24. K.C. Narang and S.K. Chopra, "Studies on Alkaline Activation of BF, Steel and Alloy Slags", Silicates Industrielles, Vol 9, 1983, pp. 175-182.

25. ASTM, Annual Book of ASTM Standards, Vol. 04.01 Cement; Lime; Gypsum, 1992.

26. E. Douglas *et al*, "Determination of Glass Content in Fly ashes and Blast Furnace Salgs", Canmet Report NO. 85-6E, 1985.

27. K. Aihara, "Particle Growth Characteristics of Active MgO", Master of Science Thesis, Department of Metallurgy, University of British Columbia, January, 1973.

28. H.F.W. Taylor, Cement Chemistry, Academic Press Limited, London, 1990.

APPENDIX I

Table I - 1 Average Compressive Strength of Blended Cements

Lot PC	Portland Cement
Lot A	90% PC/10% Slag
Lot B	80% PC/20%Slag
Lot C	45% PC/45% Slag/10% Gypsum
Lot D	40% PC/25%Slag/25%BFSlag/10%Gypsum
Lot E	10% PC/40%Slag/40%BFSlag/10%Gypsum

Average Strength (MPa) - First Series

DAYS	PC	A-1	A-2	A-3	C-1	C-2	C-3
1	5.1	9.6	14.9	7.8	3.9	4.7	4.4
7	36.6	58.5	57.2	52.2	17.0	14.5	18.3
14	44.4	68.6	65.7	65.3	24.6	24.2	26.2
35	52.8	73.7	76.7	72.8	37.0	32.1	37.0
DAYS	PC	D-1	D-2	D-3	E-1	E-2	E-3
1	5.1	4.3	4.2	4.5	1.4	3.5	5.1
7	36.6	18.2	18.1	20.6	7.8	8.9	17.6
14	44.4	22.8	24.0	23.6	9.3	15.5	19.5
35	52.8	27.9	25.4	38.0	13.1	18.3	23.9

Averages Stength (MPa) - Second Series

DAYS	PC	A-1	A-2	B-1	B-2
1	12.2	21.4	21.2	14.7	12.5
7	53.9	60.3	69.7	52.7	52.1
14	55.7	61.7	71.2	64.1	79.2
35	61.0	68.2	80.0	69.6	72.4

Table I - 2 Compressive Applied Loads

Lot PC	Portland Cement
Lot A	90% PC/10% Slag
Lot B	80% PC/20%Slag
Lot C	45% PC/45% Slag/10% Gypsum
Lot D	40% PC/25%Slag/25%BFSlag/10%Gypsum
Lot E	10% PC/40%Slag/40%BFSlag/10%Gypsum

		Strength (lbs-force)			
	Sample #	1 day	7 day	14 day	35 day
Lot PC-1	1	115	N/T	1000	1025
	2	127	N/T	1040	1400
	3	125	N/T	N/T	1600
	Average	122.3	N/T	1020.0	1341.7
Lot PC-2	1	123	960	1280	N/T
	2	160	900	1200	N/T
	3	125	N/T	N/T	N/T
	Average	136.0	930.0	1240.0	N/T
Lot A-1 #1	1	N/T	850	1100	1650
	2	N/T	820	1140	1275
	3	N/T	820	1020	1450
	Average	N/T	830.0	1086.7	1458.3
Lot A-2 #1	1	N/T	770	1150	1250
	2	N/T	960	1160	1350
	3	N/T	650	1080	1300
	Average	N/T	793.3	1130.0	1300.0
Lot A-1 #2	1	250	1700	1980	1850
	2	290	1060	1740	1900
	3	195	1700	1510	N/T
	Average	245.0	1486.7	1743.3	1875.0
Lot A-2 #2	1	375	1420	1780	2250
	2	360	1500	2250	1950
	3	400	1440	980	1650
	Average	378.3	1453.3	1670.0	1950.0
Lot A-3	1	225	1740	1600	1750
	2	215	1160	1720	1950
	3	155	1080	N/T	N/T
	Average	198.3	1326.7	1660.0	1850.0

*N/T - No test performed

Table I - 2(cont.) Compressive Applied Loads

		Strength (lbs-force)			
	Sample #	1 day	7 day	14 day	35 day
Lot C-1	1	100	400	600	1080
	2	73	400	700	760
	3	128	500	580	980
	Average	100.3	433.3	626.7	940.0
Lot C-2 #1	1	150	N/T	750	740
	2	180	N/T	660	960
	3	110	N/T	N/T	N/T
	Average	146.7	N/T	705.0	850.0
Lot C-2 #2	1	100	385	525	900
	2	80	345	530	740
	3	90	375	N/A	700
	Average	90.0	368.3	527.5	780.0
Lot C-3 #1	1	100	N/T	770	860
	2	73	N/T	550	860
	3	128	N/T	760	1340
	Average	100.3	N/T	693.3	1020.0
Lot C-3 #2	1	120	385	610	900
	2	140	540	710	720
	3	115	470	600	960
	Average	125.0	465.0	640.0	860.0

Table I - 2(cont.) Compressive Applied Loads

		Strength (lbs-force)			
	Sample #	1 day	7 day	14 day	35 day
Lot D-1	1	120	500	560	760
	2	105	425	610	790
	3	103	N/T	570	580
	Average	109.3	462.5	580.0	710.0
Lot D-2	1	106	520	530	660
	2	127	400	690	660
	3	88	N/T	N/T	620
	Average	107.0	460.0	610.0	646.7
Lot D-3	1	120	520	500	840
	2	102	510	700	1020
	3	123	545	600	1040
	Average	115.0	525.0	600.0	966.7
Lot E-1	1	50	195	220	350
	2	30	200	270	315
	3	30	N/T	220	N/T
	Average	36.7	197.5	236.7	332.5
Lot E-2	1	105	245	360	465
	2	73	210	460	510
	3	90	N/T	360	420
	Average	89.3	227.5	393.3	465.0
Lot E-3	1	145	440	540	560
	2	152	415	490	620
	3	90	485	460	640
	Average	129.0	446.7	496.7	606.7

Table I - 2(cont.) Compressive Applied Loads

		Strength (lbs-force)			
	Sample #	1 day	7 day	14 day	35 day
Lot PC-3	1	225	1220	1500	1550.0
	2	290	1310	1330	N/T
	3	280	1580	N/T	N/T
	Average	265.0	1370.0	1415.0	1550.0
Lot A-1 #3	1	590	1400	1510	1420
	2	460	1560	1630	2050
	3	585	1640	N/T	N/T
	Average	545.0	1533.3	1570.0	1735.0
Lot A-2 #3	1	615	1900	1790	2220
	2	555	1600	1660	2100
	3	450	1820	1980	1780
	Average	540.0	1773.3	1810.0	2033.3
Lot B-1	1	300	1390	1630	1770
	2	415	1430	N/T	N/T
	3	405	1200	N/T	N/T
	Average	373.3	1340.0	1630.0	1770.0
Lot B-2	1	305	1330	1740	1740
	2	315	1320	2020	1940
	3	330	N/T	2060	N/T
	Average	316.7	1325.0	1940.0	1840.0

* Second series of compression samples